AD-A080 092 SOUTHWEST RESEARCH INST SAN ANTONIO TEX F/G 20/1
RESEARCH AND DEVELOPMENT OF NMR METHODS FOR THE NONDESTRUCTIVE --ETC(U)
DEC 79 G A MATZKANIN F44620-76-C-0114
UNCLASSIFIED AFOSR-TR-80-0106 NL

| OF |
AD A
080092

END
DATE
FILMED
2 — 80
DDC

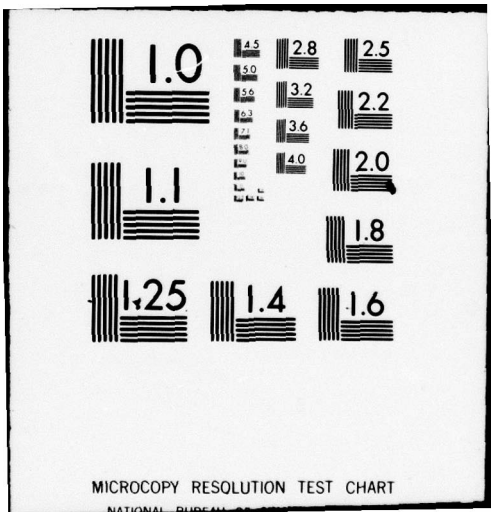
1.0
1.1
1.25
1.4
1.6
1.8
2.0
2.2
2.5
2.8
3.2
3.6
4.0
4.5
5.0
5.6
6.3
MICROCOPY RESOLUTION TEST CHART

AFOSR-TR- 80-0106

RESEARCH AND DEVELOPMENT OF NMR METHODS FOR THE NONDESTRUCTIVE CHARACTERIZATION OF INTERNAL STRESS AND STRAIN IN NONFERROMAGNETIC STRUCTURAL MATERIALS

by

G. A. Matzkanin

LEVEL II

FINAL TECHNICAL REPORT
SwRI Project No. 15-4580

prepared for

Air Force Office of Scientific Research
Directorate of Electronic and Solid State Sciences
Contract F44620-76-C-0114
Project No. 9761-02

December 1979

Research Sponsored by Air Force Office of Scientific Research
Directorate of Electronic and Solid State Sciences
"Approved for public release; distribution unlimited."

SOUTHWEST RESEARCH INSTITUTE
SAN ANTONIO HOUSTON

UNCLASSIFIED

SECURITY CLASSIFICATION OF THIS PAGE (When Data Entered)

REPORT DOCUMENTATION PAGE	READ INSTRUCTIONS BEFORE COMPLETING FORM
1. REPORT NUMBER: AFOSR-TR-80-0166	2. GOVT ACCESSION NO. / 3. RECIPIENT'S CATALOG NUMBER
4. TITLE (and Subtitle): Research and Development of NMR Methods for the Nondestructive Characterization of Internal Stress and Strain in Nonferromagnetic Structural Materials	5. TYPE OF REPORT & PERIOD COVERED: Final Technical Report. 1 Jun 76 – 31 Oct 79
	6. PERFORMING ORG. REPORT NUMBER: 15-4580
7. AUTHOR(s): G. A. Matzkanin	8. CONTRACT OR GRANT NUMBER(s): F44620-76-C-0114
9. PERFORMING ORGANIZATION NAME AND ADDRESS: Southwest Research Institute / 6220 Culebra Rd., P. O. Drawer 28510 / San Antonio, TX 78284	10. PROGRAM ELEMENT, PROJECT, TASK AREA & WORK UNIT NUMBERS: 2306/A2 / 61102F / Project No. 9761-02 / A2
11. CONTROLLING OFFICE NAME AND ADDRESS: AFOSR/NE / Bldg. 410, Bolling AFB, D. C. 20332	12. REPORT DATE: 31 Dec 79
	13. NUMBER OF PAGES: 61
14. MONITORING AGENCY NAME & ADDRESS (if different from Controlling Office)	15. SECURITY CLASS. (of this report): UNCLASSIFIED
	15a. DECLASSIFICATION/DOWNGRADING SCHEDULE

16. DISTRIBUTION STATEMENT (of this Report)

Approved for public release; distribution unlimited.

17. DISTRIBUTION STATEMENT (of the abstract entered in Block 20, if different from Report)

18. SUPPLEMENTARY NOTES

19. KEY WORDS (Continue on reverse side if necessary and identify by block number)

Nondestructive Evaluation, Residual Stress, Plastic Deformation, Internal Strain, Nuclear Magnetic Resonance, Nuclear Acoustic Resonance, Aluminum, Superalloys

20. ABSTRACT (Continue on reverse side if necessary and identify by block number)

Two new nondestructive evaluation (NDE) methods for measuring residual stress in non-ferromagnetic metals have been investigated, namely, inductive nuclear magnetic resonance (NMR) and nuclear acoustic resonance (NAR). In metals, NMR is restricted to the surface by the electromagnetic skin effect while NAR is sensitive to the interior of the specimen as well as the surface. Results of NAR experiments on plastically deformed polycrystalline aluminum specimens were very encouraging. The NAR signature was found to vary with degree of plastic deformation in agreement with published NMR theory based on strain-induced

DD FORM 1 JAN 73 1473

UNCLASSIFIED 328 200

SECURITY CLASSIFICATION OF THIS PAGE (When Data Entered)

quadrupole interactions. Shapes of the NAR signals from deformed aluminum were found to depend on the magnetic modulation frequency; it is suggested that this modulation dependence could form the basis for determining distributions of internal stress and strain in metals. Pulsed NMR experiments on bulk aluminum specimens were complicated by large electromagnetically generated acoustic transient signals not associated with nuclear resonance. Digital subtraction signal processing was used to discriminate against the spurious signals; however it did not separate NMR signals from the electromagnetically generated transients. Pulsed NMR signals observed from aluminum in a powdered specimen of the superalloy IN-100 provides a basis for considering NMR and NAR for nondestructive measurements in this important class of alloys.

TABLE OF CONTENTS

	Page
LIST OF ILLUSTRATIONS	ii
SUMMARY	iv
I. INTRODUCTION	1
II. INDUCTIVE NMR	3
A. Experimental Approach	3
B. Results on Bulk Aluminum Specimen	3
C. Results on IN-100 Superalloy	16
III. ACOUSTIC NMR	21
A. Specimens	21
B. Experimental Approach	21
C. Results on Plastically Deformed Aluminum Specimens	23
1. Linewidth vs. Strain	23
2. Lineshape vs. Strain	27
3. Separation of Experimentally Observed NAR Signals into χ' and χ'' Components	29
4. Modulation Effects	33
D. Additional Results	33
1. Aluminum Copper Alloys	33
2. NAR Using Electromagnetic Acoustic Generation	35
IV. DISCUSSION	39
V. CONCLUSIONS AND RECOMMENDATIONS	41
VI. SUPPLEMENTARY INFORMATION	42
A. Publications	42
B. Personnel	42
C. Coupling	42
VII. REFERENCES	43
APPENDIX	A-1

LIST OF ILLUSTRATIONS

Figure	Title	Page
1	Electromagnetic NMR Approach	4
2	Block Diagram of Pulsed Inductive NMR Approach	5
3	Transient Responses in Aluminum Following Application of an RF Pulse	7
4	Free Induction Decays from Large Aluminum Particles and Foil	8
5	Field Dependence of the Spurious Transient Signal Amplitude	9
6	Block Diagram of Pulsed Inductive NMR Approach Incorporating Digital Subtraction	11
7	Reconstructed RF Signals from HMT and NH_4NO_3	12
8	NMR Signals From NH_4NO_3	13
9	Illustration of Digital Subtraction Technique for 26 Micron Aluminum Powder	14
10	Illustration of Digital Subtraction Technique for Aluminum Particles (0.84mm to 2.38mm)	15
11	Illustration of Digital Subtraction Technique Applied to a 1/2 in.-diameter Aluminum Cylinder	17
12	Pulsed NMR Signals from Aluminum in the IN-100 Superalloy	19
13	Signal Averaged Free-Induction-Decay from Aluminum in the IN-100 Superalloy	20
14	Block Diagram of Nuclear Acoustic Resonance Approach	22
15	Dependence of Aluminum Acoustic Absorption First Derivative on Compressive Strain	24
16	Schematic Representation of Admixture of χ' and χ''	25
17	Comparison of Theoretical Strain-Broadened Lineshape with Gaussian Function	30
18	Computer Extracted χ' and χ'' Components from Experimental NAR Signals for 5% Tensile Strained Aluminum	32
19	Effect of Modulation Frequency on NAR Lineshape as a Function of Plastic Deformation in Polycrystalline Aluminum	34

LIST OF ILLUSTRATIONS (continued)

Figure	Title	Page
20	^{27}Al Acoustic NMR Signals from Two Al-Cu Alloys	36
21	Schematic Illustration of Electromagnetic Generation of Longitudinal Acoustic Standing Waves in Aluminum Cylinder	37
22	Ultrasonic Standing Wave Spectrum Generated in an Aluminum Cylinder by EMAT in Frequency Range of 9 MHz to 11 MHz	38

SUMMARY

The important roles played by residual stresses and internal strains in determining the service behavior of metallic components and structures are well-documented, but the need for nondestructive evaluation of stress and strain was only recently underscored at the 1975 Air Force Workshop on Nondestructive Evaluation of Residual Stress. At this workshop it was emphasized that although research is well underway on several promising methods for measuring residual stress in magnetic metals, no comparable level of research is being conducted on methods suitable for residual stress measurement in non-ferromagnetic metals with the exception of X-ray diffraction and possibly differential acoustic velocimetry. Thus, a high priority was assigned to develop measurement methods suitable for application to non-ferromagnetic metals such as aluminum alloys and superalloys.

The purpose of this research program was to investigate two new nondestructive evaluation methods for measuring residual stress in non-ferromagnetic metals: inductive nuclear magnetic resonance (NMR) and nuclear acoustic resonance (NAR). Both methods are closely related and in principle are applicable to metals and non-metals. However, in metals, inductive NMR is restricted to the surface by the electromagnetic skin effect while NAR is sensitive to the interior of the specimen as well as the surface.

Based on the results of this program, inductive NMR does not appear promising at this time because of complications introduced by application of a pulsed radio frequency voltage to a bulk metal resulting in large transient signals not associated with nuclear resonance. These transient signals observed in experiments conducted on aluminum cylinders were shown to be acoustic in origin and to increase in amplitude with increasing magnetic field. They are analogous to the acoustic signals generated electromagnetically with an electromagnetic acoustic transducer (EMAT). Digital subtraction signal processing was used to discriminate against the spurious signals; however, it did not separate NMR signals from the ultrasonically generated transients.

On the other hand, results of NAR experiments on plastically deformed polycrystalline aluminum specimens were very encouraging. In fact the first report of NAR signals obtained from a polycrystalline metal, aluminum, was made during the course of this research. Observed signatures are comparable in amplitude and shape to NAR signals previously reported for single crystal specimens, and the NAR signature was found to vary with degree of plastic deformation in agreement with published NMR theory based on strain-induced quadrupole interactions. Although present theory is applicable only to inductive NMR, results presented in this report indicate that the basic concepts are also applicable to NAR. Successful modification of the NMR theory and subsequent experimental verification should provide a foundation for interpreting NAR signatures quantitatively in terms of the sense and degree of deformation. Shapes of the NAR signals from deformed aluminum are dependent on the modulation frequency of the magnetic field used for detection. Since the penetration of the modulated field depends on frequency, it is suggested that this shape dependence could form the basis for utilizing NAR to determine the distribution of internal stress and strain in metals.

In addition to the NAR experiments on deformed aluminum, other limited studies relevant to development of NAR and NMR for practical application were conducted. The feasibility of detecting NAR signals in aluminum-copper alloys and the generation of acoustic standing waves in an aluminum cylinder using an EMAT were demonstrated. Pulsed inductive NMR signals were observed from the aluminum constituent in a powdered specimen of the nickel-base superalloy, IN-100. This observation provides the basis for further consideration of NMR and NAR applied to nondestructive measurements in this important class of metals.

In summary the results obtained in this program indicate that NAR has potential for the nondestructive determination of residual stress in non-ferromagnetic metals. Additional NAR experiments should be conducted and available theory suitably modified to provide a more complete understanding of the effect of strain-induced quadrupole perturbations on NAR signatures. Results obtained to date, demonstrate that it should be possible to quantitatively relate characteristics of the NAR signature to internal stress and strain. Further work is also recommended for applying NAR to superalloys.

I. INTRODUCTION

The importance of the residual stress problem to the Air Force was emphasized at a workshop on Nondestructive Evaluation of Residual Stress held in San Antonio, Texas in August, 1975.[1] In air frame structural metals, residual stresses are commonly associated with inhomogeneous plastic deformation. Metal-working processes such as cutting, forging, drawing, rolling, etc., induce residual stresses. In addition, the residual stresses associated with fatigue cracks play an important role in crack initiation and propagation and sudden catastrophic failure of service components. An extremely important problem relevant to the Air Force is that of low-cycle fatigue cracks in gas turbine engine discs fabricated from nickel-base super alloys. Methods to detect and quantitatively characterize such cracks is pacing the development of "retirement for cause" strategies based on fracture mechanics analyses of these critical engine components.[2] Residual stress information is important in developing a complete fracture mechanics analysis so that a sound basis will be established for service-life extensions of one or more overhaul periods.

Lacking adequate nondestructive residual stress measuring methods, the traditional approach to achieving an acceptable level of structural safety has been to design for large safety factors. Development of capabilities to nondestructively measure residual stress could aid in design of more efficient and reliable structures and components, and also improve means of assessing fabrication or service-induced changes in stresses. Clearly, such capabilities would be valuable in reducing over-design and extending life of critical components, thereby conserving material resources while simultaneously improving performance.

Currently the most widely used, completely nondestructive method for determining internal lattice strain in metals is X-ray diffraction; however, this approach is limited to the depths of penetration of the X-rays and is also subject to difficulties of interpretation as, for example, in multi-phase systems.[3] X-ray diffractometers designed expressly for residual stress measurement are commercially available; however, the method is limited to surface measurement and the accuracy decreases with cold work. The method is not applicable to all materials and the size, complexity, time-required-for-use, and cost of instrumentation, though greatly improved over the past few years, have severely restricted its application.

For ferromagnetic materials (e.g. structural steels) residual stress measurement methods based on magnetic properties exist and are being refined and applied to a limited extent.[4] In nonferromagnetic materials, however, apart from X-ray diffraction, no completely nondestructive method for residual stress measurement is available. New methods which have been suggested and explored to some extent include acoustic birefringence,[5] Mossbauer effect spectroscopy,[6] shifts in characteristic X-ray line profiles,[7] positron annihilation,[8] ultrasonic measurements,[9] and nuclear magnetic resonance.[10]

The work reported herein, performed under Contract No. F44620-76-C-0114, was directed toward the investigation and development of

inductive nuclear magnetic resonance (NMR) and nuclear acoustic resonance (NAR) for the purpose of residual stress measurement in nonferromagnetic materials. These two methods are closely related and, in principle, are applicable to metals and nonmetals. However, in metals, electrical conductivity limits conventional inductive NMR methods to the electromagnetic skin depth which is typically 10 to 100 μm at the radio frequencies employed. NAR on the other hand, circumvents the skin depth limitation in metals and is, therefore, sensitive to the interior of the specimen as well as the surface. Despite the limitation of inductive NMR to the skin depth, investigation of this method was pursued in addition to NAR because of potential applications for the measurement of surface stresses. In addition, the field of NAR has not yet reached the level of maturity of NMR, and prior to this work, had been investigated only in single crystals to obtain detailed information on crystal orientation dependence.(11)

The primary objectives of the work reported herein were to investigate the effects of strain and plastic deformation on NMR and NAR in bulk metals and alloys to provide a basis for applying these techniques to the nondestructive characterization of internal stress and strain. Results of the inductive NMR work are presented in Section II, while the NAR results are presented in Section III. A discussion of the results is presented in Section IV. Conclusions and recommendations for further work are presented in Section V and supplementary information on publications, personnel and coupling activities is presented in Section VI. References are listed in Section VII. Background information on the basic principles of NMR and the effect of strain is given in the Appendix.

II. INDUCTIVE NMR

A. Experimental Approach

Experimental techniques for NMR are well-documented in the literature[12,13] so only a brief description of the specific experimental procedures utilized during this program will be presented. Both NMR and NAR involve the resonant excitation of atomic nuclei having magnetic moments. A magnetic field externally applied to the specimen polarizes the nuclear magnetic dipole system which is then excited with radio frequency (rf) energy at the appropriate frequency for resonant interaction. The resonance frequency is proportional to the intensity of the applied magnetic field. For typical materials, magnetic fields of 1 T (10^4G) correspond to frequencies of about 1 MHz. In the conventional NMR approach, resonance excitation and detection are accomplished by inductively coupling the specimen to an rf oscillator by means of an induction coil which encircles the specimen, as shown schematically in Figure 1.

Inductive NMR may be classified as either continuous wave (CW) or transient (pulsed). CW NMR involves excitation of the specimen with rf energy while slowly sweeping either the applied magnetic field or the rf frequency through the resonance condition. In pulsed NMR, a short burst of rf is applied to the specimen at the nuclear resonance frequency after which the response of the nuclear magnetic dipole system is monitored by means of signals induced in a detecting coil. The signals observed are either free induction decays or spin echos.[14] In the inductive NMR work discussed in this report, pulsed NMR was utilized since it is faster and generally contains more information in the signal parameters than the CW approach.

A block diagram of the pulsed NMR apparatus utilized is shown in Figure 2. The system is composed of seven principal components: (1) digital rf exciter, controller and repetition rate generator; (2) transmitter; (3) transmit/receive switch and matching network; (4) receiver; (5) sample coil; (6) display unit; and (7) magnet. In the system described here the rf exciter provides a 10 MHz output which is crystal-controlled for frequency stability. Two rf pulses are available which can be varied in duration to provide either 90° or 180° rotation of the nuclear magnetization. The phase relationship between the two pulses can be switch-selected to be 0° or 90°. The transmitter consists of transistor amplifiers and a vacuum tube amplifier which is capable of producing rf pulse amplitudes of 500V peak-to-peak across 50 ohm load. This 5 kW of power provides a 10 μs, 90° pulse and a 20 μs 180° pulse in aluminum. The system receiver utilizes a dual-gate MOSFET stage to establish a low-noise figure and high-impedance input. The three stages of the receiver are synchronously tuned to 10 MHz to provide high sensitivity and good signal-to-noise ratio.

B. Results on Bulk Aluminum Specimen

The major inductive NMR effort was directed toward obtaining useable pulsed NMR signals from bulk metal specimens. The difficulty lies in the spurious signals produced when a large metal specimen in

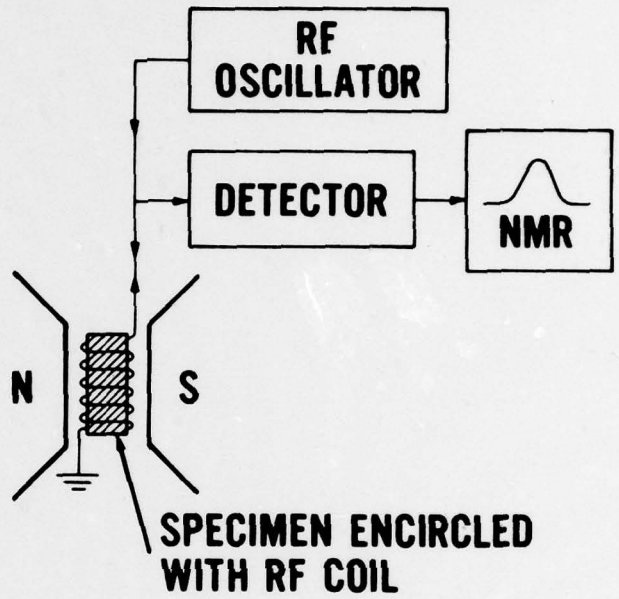

3369

FIGURE 1. ELECTROMAGNETIC NMR APPROACH

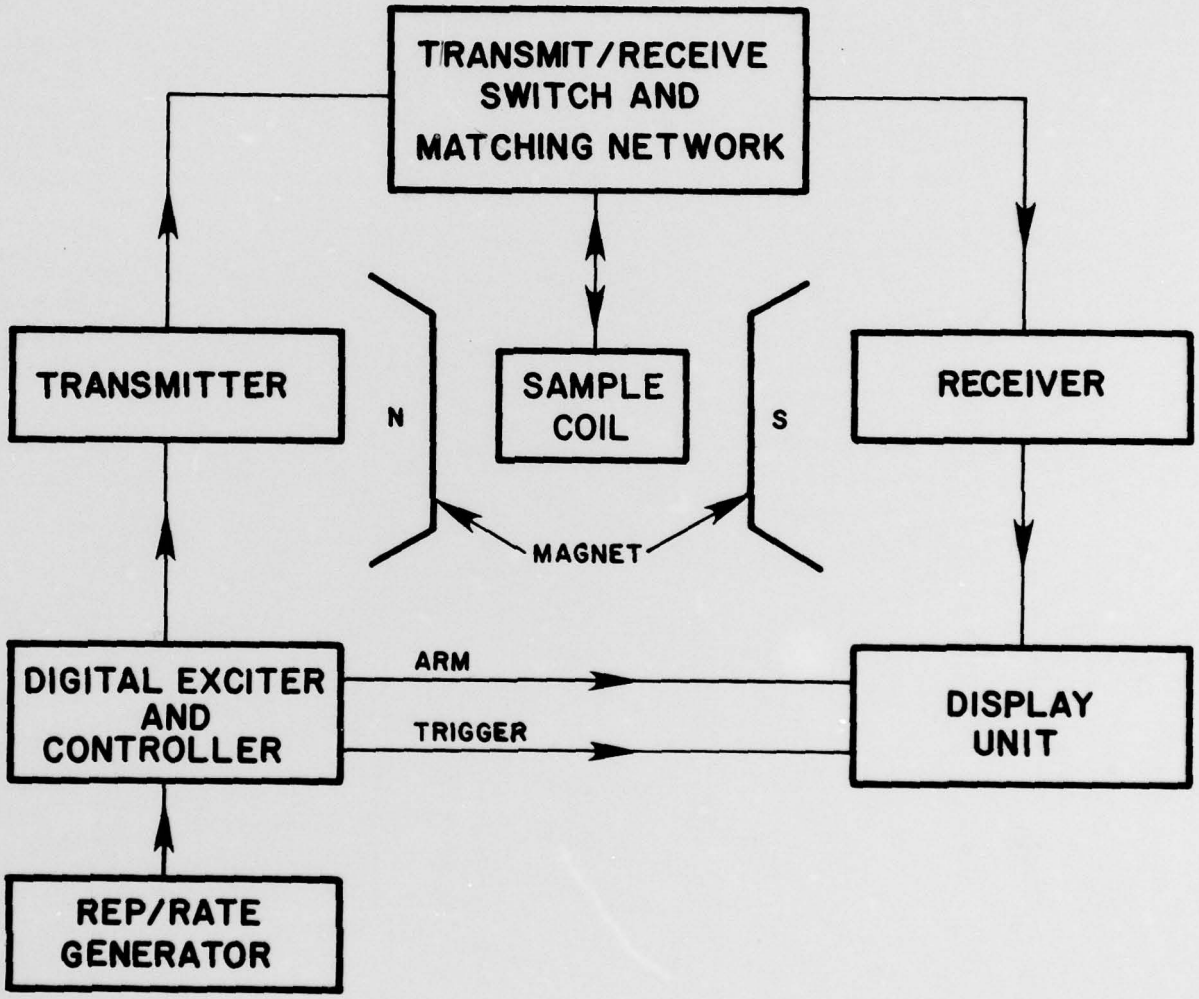

FIGURE 2. BLOCK DIAGRAM OF PULSED INDUCTIVE NMR APPROACH

a magnetic field is subjected to an rf pulse. Spurious transient signals following application of an rf pulse have been reported by a number of investigators, but their origins are not fully understood at this time.[15] It is thought that they are caused by acoustic modes shock-excited by the rf pulses, and circulating eddy currents. The spurious signals tend to be very large in amplitude and long-lasting compared with signals of nuclear origin. An example of these signals is illustrated in Figure 3a which shows the spurious transient response observed from a 1.27 cm (0.5 in.)-diameter cylindrical specimen of aluminum. In contrast, the nuclear free induction decay (FID) observed from aluminum powder is shown in Figure 3b. Note that the time duration of the spurious transient response from the aluminum cylinder is quite long and tends to mask any observable nuclear signal. In addition, the NMR signal from bulk aluminum is expected to be very weak because of the relatively small number of nuclei in the skin depth surface layer. To further explore the effect of sample size on pulsed NMR signals, experiments were conducted on aluminum particles ranging in size from 50 to 150 μm. These particles are larger than the aluminum skin depth (approximately 40 μm at 10 MHz) and were expected to exhibit a spurious signal. Figure 4a shows the results from these particles. The NMR signal from the particles is somewhat lower in intensity than for the 26 μm powder shown in Figure 3b. This is because all of the nuclei contribute to the NMR signal from the 26 μm powder whereas fewer nuclei contribute to the signal from the larger particles since the particles are not completely penetrated by the rf field. Analysis of the signal also indicates the presence of a spurious response although not as large as that observed for the bulk aluminum cylinder. A signal obtained from a specimen of aluminum foil is shown in Figure 4b. In this case the specimen was approximately 60 μm thick, 2.54 cm (1 in.) wide and 5.08 cm (2 in.) long. It was wrapped around the inside of a glass sample vial, leaving about a 0.32 cm (0.125 in) gap between the ends. This gap avoided having a shorted turn of conductive material inside the rf coil, thereby reducing eddy current responses. As can be seen, a transient signal was observed very similar to that obtained from the larger aluminum particles (Figure 4a). Since the thickness of the foil corresponds approximately with the skin depth of aluminum, it should be indicative of the NMR signal expected from bulk (larger than skin depth) specimens. However, as indicated earlier, spurious signals present additional difficulties in the detection of NMR signals from bulk metal specimens.

The characteristics of the spurious signals were investigated by examining the field-dependence for transient signals from an aluminum cylinder. The signal amplitude was found to depend linearly on the square of the applied magnetic field over a wide field range as shown in Figure 5. Other investigators have shown both experimentally and theoretically that transient responses associated with electromagnetically excited acoustic modes depend quadratically on the applied field[16] and the graph shown in Figure 5 is consistent with these results. Thus this result is interpreted as a strong indication that the spurious signals are acoustic in origin. Additional evidence for concluding that the spurious signals are acoustic in origin was obtained by examining the oscillation frequency of the spurious transient signals. Although the transient response seems to be a complex combination of signals, the dominant frequency of approximately 90 kHz is comparable to the frequency of acoustic standing shear waves in a 1.27 cm (0.5 in.)-long aluminum

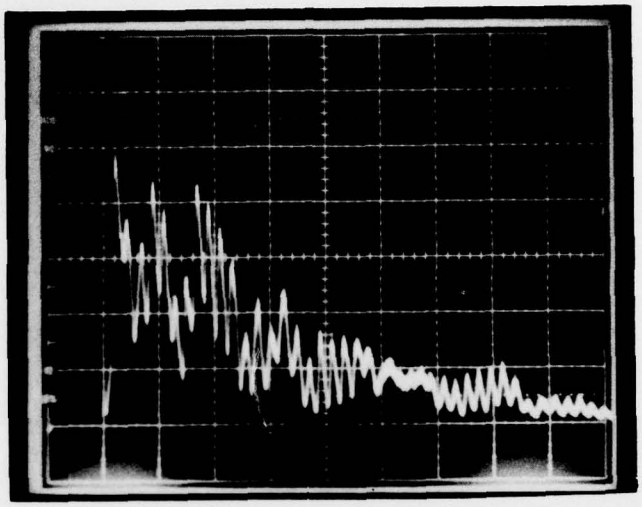

V - 2V/div

H - 50 μs/div

a. 1/2-in. Diameter Aluminum Cylinder

5197

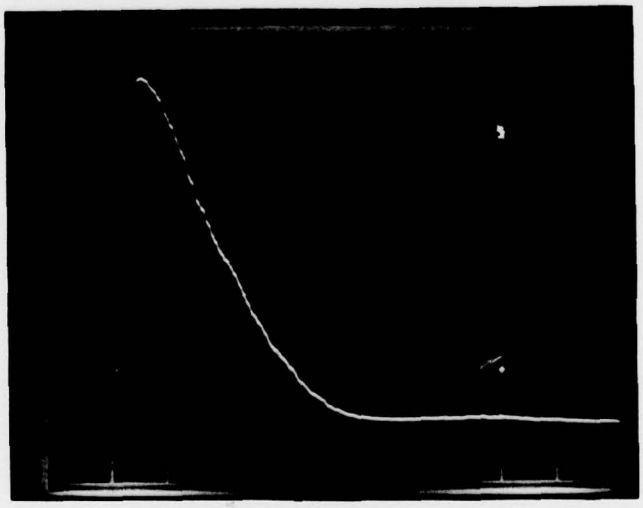

V - 1V/div

H - 20 μs/div

b. 26 Micron Aluminum Powder

FIGURE 3. TRANSIENT RESPONSES IN ALUMINUM FOLLOWING APPLICATION OF AN RF PULSE

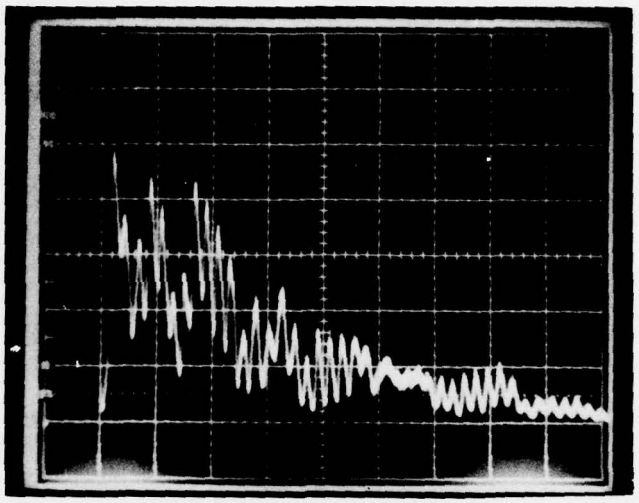

V - 2V/div

H - 50 μs/div

a. 1/2-in. Diameter Aluminum Cylinder

5197

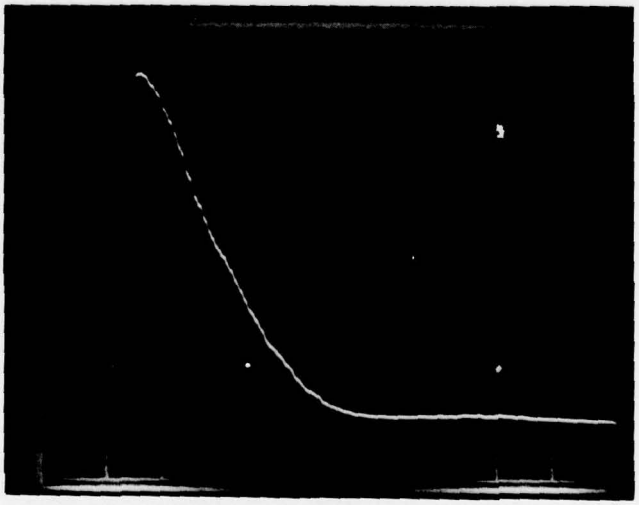

V - 1V/div

H - 20 μs/div

b. 26 Micron Aluminum Powder

FIGURE 3. TRANSIENT RESPONSES IN ALUMINUM FOLLOWING APPLICATION OF AN RF PULSE

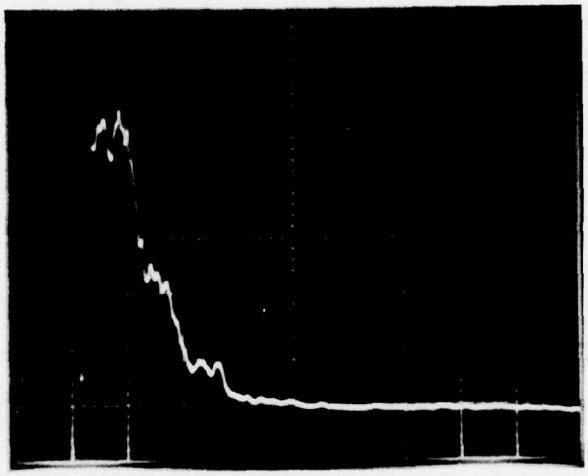

V - 0.1V/div

H - 20 μs/div

a) 100 micron particles

4345

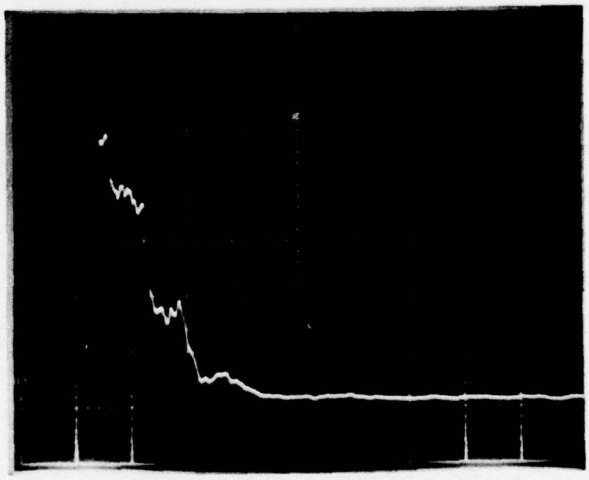

V - 0.1V/div

H - 20 μs/div

b) 60 micron-thick foil

FIGURE 4. FREE INDUCTION DECAYS FROM LARGE ALUMINUM PARTICLES AND FOIL

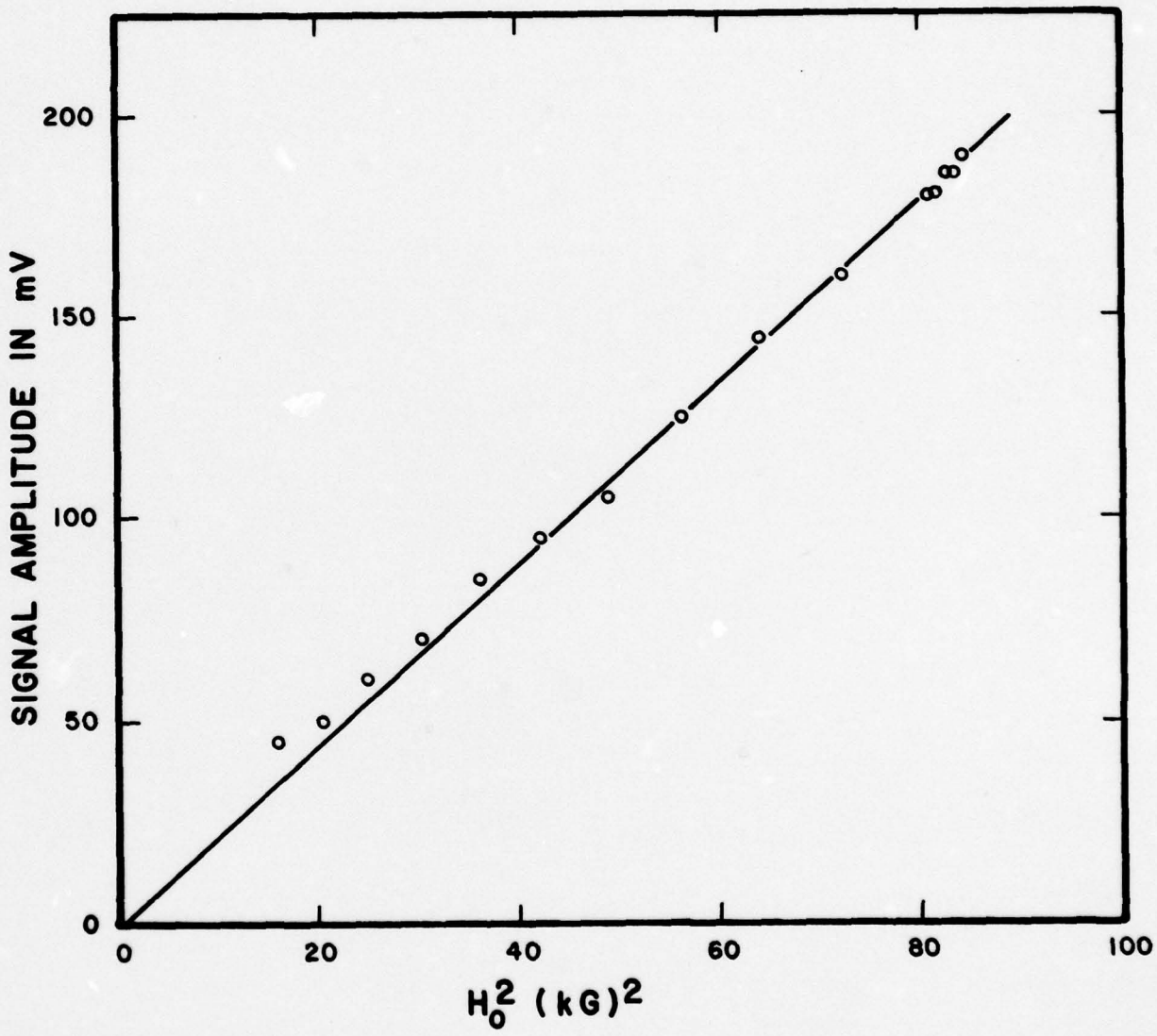

5009

FIGURE 5. FIELD DEPENDENCE OF THE SPURIOUS TRANSIENT SIGNAL AMPLITUDE

cylinder which is 120 kHz. Because of the specimen and rf coil geometry, it is likely that electromagnetically generated acoustic signals are not pure shear waves, but rather complex combinations of modes.

In order to discriminate against various transient signals and thereby permit observation of inductive NMR signals in bulk metal samples an electronic cancellation method utilizing digital techniques was investigated. A block diagram of the circuit is shown in Figure 6. Basically, the approach involves obtaining the difference between two digitized transient responses following application of an rf pulse, one at the precise field for nuclear resonance and the other at a different field value. The digitized signals are stored in memory and then subtracted to provide a difference signal. The "off resonance" response is obtained at a magnetic field far enough away from the resonance field so that no NMR component is present, but close enough to the resonance field that the spurious component is essentially unchanged. Thus the difference between the two responses should result in only the NMR component.

The effectiveness of the digital subtraction approach was evaluated in an experiment involving a non-metallic specimen of $NH_4 NO_3$. An ultrasonic signal simulating a spurious component was produced by utilizing a specimen of crystalline hexamethylenetetramine (HMT). Unlike the spurious signals in bulk aluminum which were found to depend quadratically on magnetic field, the ultrasonic signals produced in HMT by the piezoelectric effect were independent of magnetic field in the range of 54 to 60 mT (540 to 600 G). The rf ultrasonic signal obtained from the HMT at a magnetic field of 60 mT (600 G) is shown in Figure 7a. (The illustrations shown in Figures 7 through 10, with the exception of 9a, are the reconstructed analog rf envelopes after digital processing.) In Figure 7b is shown the combined ultrasonic signal from HMT and the hydrogen NMR signal from a specimen of $NH_4 NO_3$ at 54 mT (540 G). When the ultrasonic signal is digitally subtracted from the combined signal, the difference shown in Figure 8a is obtained. For comparison, the NMR signal at 54 mT (540 G) obtained from $NH_4 NO_3$ with no ultrasonic signal present is shown in Figure 8b. The agreement between Figures 8a and 8b is seen to be very good and indicative of the potential use of this approach for extracting an NMR signal obscured by the presence of an interfering spurious signal.

The effectiveness of the digital subtraction approach for metallic specimens is illustrated in Figure 9 for 26 μm aluminum powder. Because of the limited range of the transient recorder used, only the first 20 μs of the FID could be digitized as shown in Figure 9a. The time delay on the transient recorder was adjusted so that signal processing was initiated just prior to the beginning of the FID. Figure 9b shows the reconstructed rf envelope of the initial portion of the 26 μm aluminum FID after digital processing. Figure 9c shows the difference signal resulting from subtracting two powdered aluminum FID's without changing the magnetic field. The difference displayed in Figure 9c is essentially zero (the upward- and downward-going "spikes" observed in the Figure are due to random noise associated with the two subtracted FID's).

Digital subtraction results for a sample of large aluminum particles (in the range of 0.84 to 2.38 mm diameter) are shown in Figure 10. These particles are considerably larger than the 40-μm

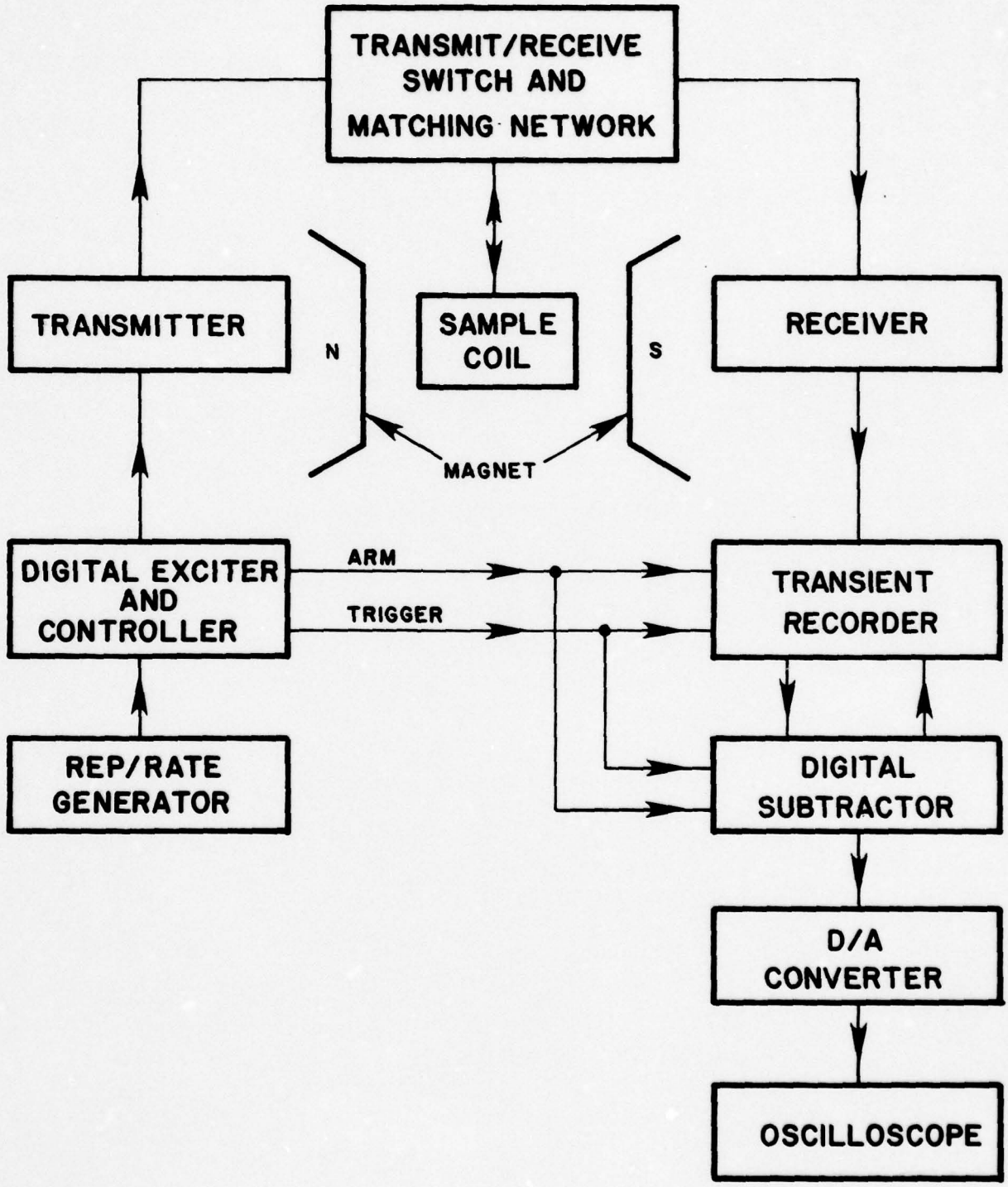

5199

FIGURE 6. BLOCK DIAGRAM OF PULSED INDUCTIVE NMR APPROACH INCORPORATING DIGITAL SUBTRACTION

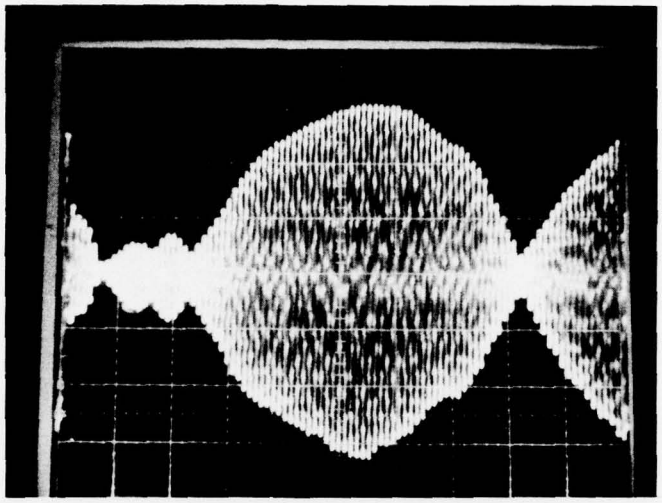

V - 1.25 V/div

H - 4 μsec/div

a. Ultrasonic Signal from Crystalline HMT at 600 Oe

4368

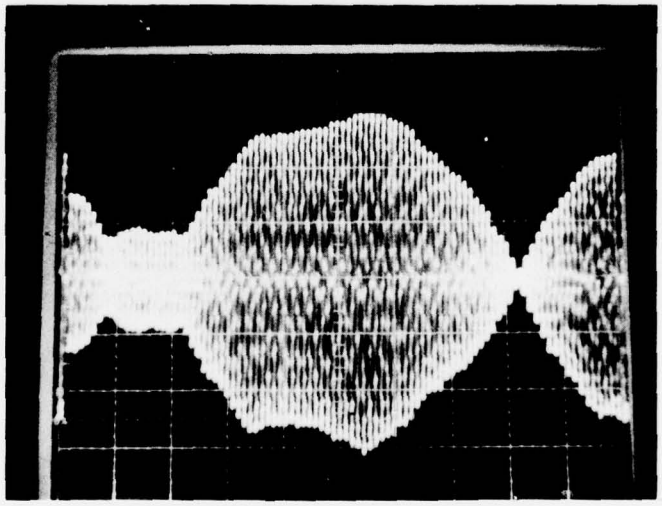

V - 1.25 V/div

H - 4 μsec/div

b. Combined Ultrasonic Signal from HMT and NMR Signal from NH_4NO_3

FIGURE 7. RECONSTRUCTED RF SIGNALS FROM HMT AND NH_4NO_3

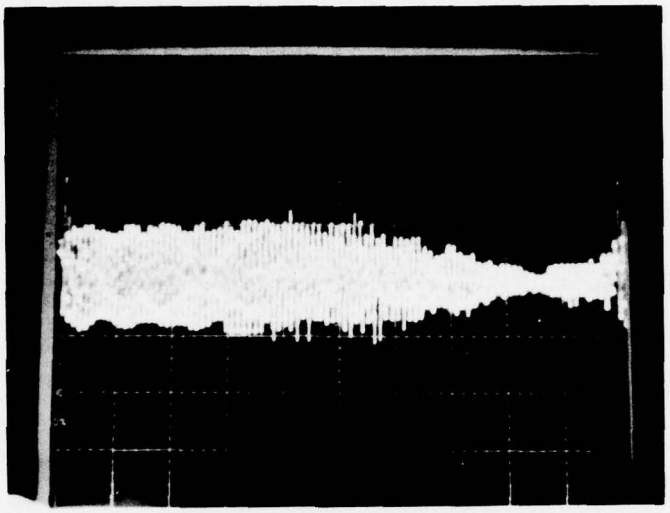

V - 1.25 V/div

H - 4 μsec/div

a. Resultant NMR Signal After Subtracting Ultrasonic Signal from Combination Signal

4370

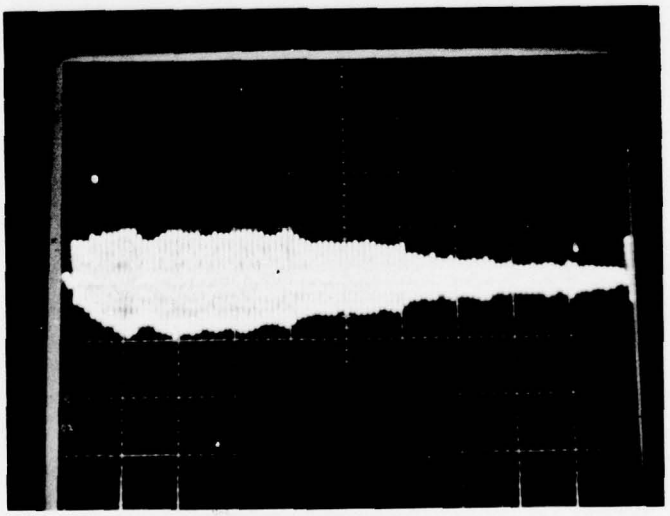

V - 1.25 V/div

H - 4 μsec/div

b. NMR Signal from NH_4NO_3 with no Ultrasonic Signal

FIGURE 8. NMR SIGNALS FROM NH_4NO_3

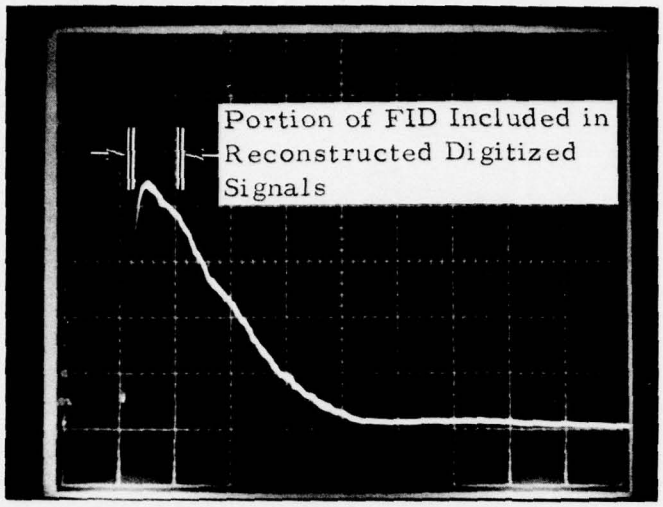

(a) Detected FID from 26 micron aluminum powder

1 V/div; 20 μs/div

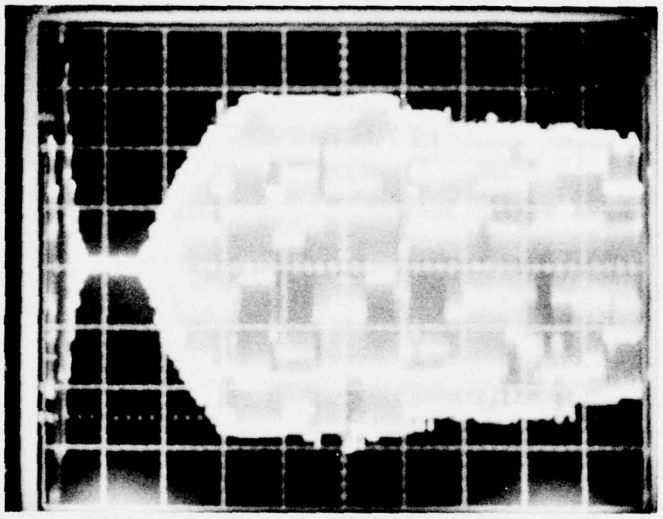

(b) Initial Portion of Reconstructed Free-Induction-Decay (FID)

1 V/div; 2 μs/div

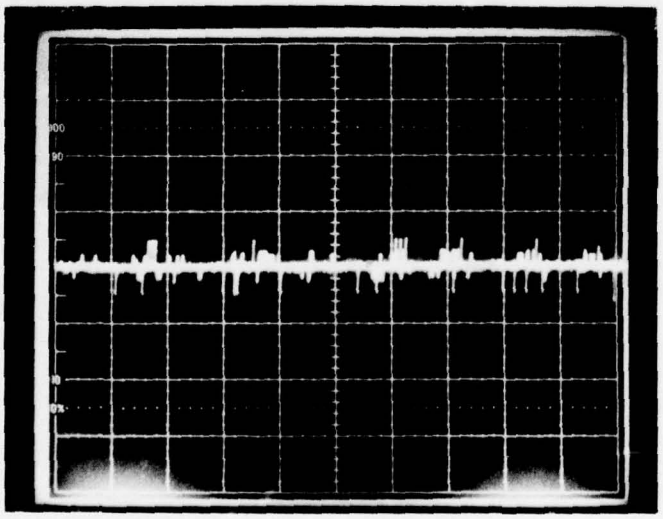

(c) Difference Signal of Two FID's at the same Magnetic Field

1 V/div; 2 μs/div

5006

FIGURE 9. ILLUSTRATION OF DIGITAL SUBTRACTION TECHNIQUE FOR 26 MICRON ALUMINUM POWDER

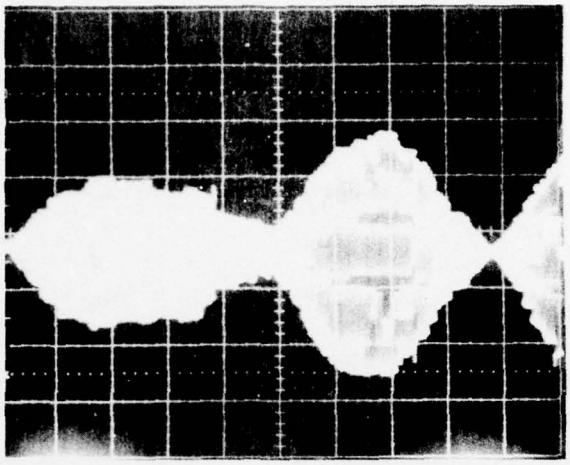

(a) Transient Response for 0.84mm to 2.38mm Aluminum Particles

1 V/div; 2 μs/div

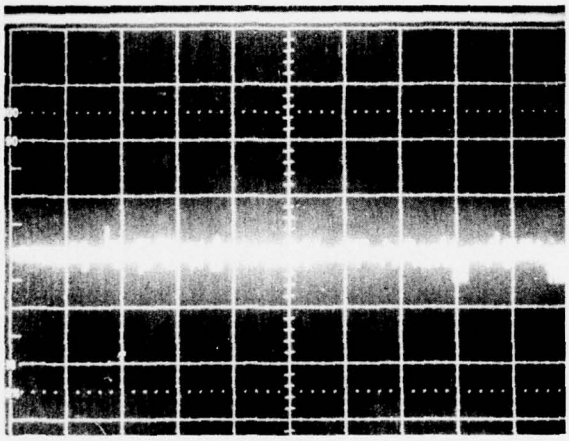

(b) Difference Signal for No Field Change

2 V/div; 2 μs/div

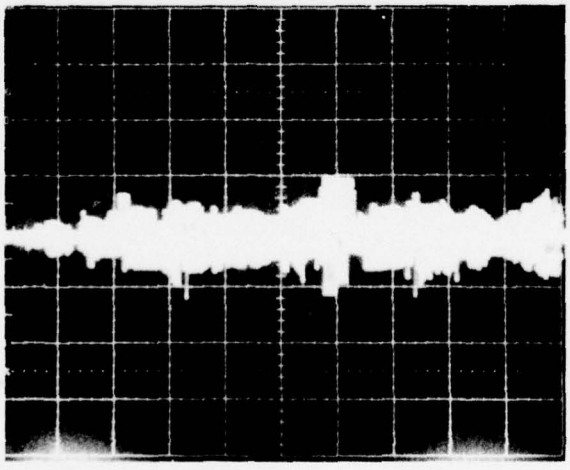

(c) Remnant NMR Signal-Difference Signal for 50 Gauss Field Change

2 V/div; 2 μs/div

5007

FIGURE 10. ILLUSTRATION OF DIGITAL SUBTRACTION TECHNIQUE FOR ALUMINUM PARTICLES (0.84mm to 2.38mm)

skin depth of aluminum, and thus it was expected that the FID would be obscured by a spurious component in the transient response. The top photograph shows the reconstructed rf signal at the nuclear resonance field comprised of both a spurious component and the NMR component. In Figure 10b is shown the difference signal for no magnetic field change; the "spikes" are due to random noise. The photograph in Figure 10c shows the difference signals obtained for a field change of approximately 5 mT (50 G). The remnant NMR signal is clearly visible in Figure 10c and illustrates the effectiveness of the digital subtraction technique for aluminum particles larger than the skin depth where the NMR signal is obscured by a spurious component.

An example of the digital subtraction approach applied to a 1.27 cm (0.5 in.)-diameter aluminum cylinder is shown in Figure 11. The top photograph shows the reconstructed rf response following a 90° pulse while the difference signal obtained from two transient responses both at the same magnetic field (corresponding to nuclear resonance) is shown in Figure 11b. This difference signal is essentially zero and comparable to that obtained for the aluminum powder (Figure 9c) and the aluminum particles (Figure 10b). The photograph in Figure 11c shows the difference signal obtained for the aluminum cylinder from two transient responses 5 mT (50 G) apart in magnetic field. As can be seen, the spurious component is completely eliminated by the digital subtraction. Unfortunately, the NMR signal from the nuclei in the skin depth of the aluminum cylinder is so weak that it is not readily observed in Figure 11c.

A number of avenues were explored for improving the NMR signal-to-noise ratio obtained with the digital subtraction technique including the utilization of signal averaging. This approach involves obtaining a number of digitally subtracted signals from a bulk aluminum specimen and adding the signals together using a signal averager. However, no signal-to-noise ratio improvements were obtained. These results are thought to be associated with the weakness of the NMR signal from a bulk specimen and the coherent nature of the spurious responses. The sensitivity of the digital subtraction technique is further reduced since the spurious response in the aluminum cylinder is dependent on the magnetic field, as shown previously in Figure 5. It thus appears that electronic signal processing does not provide adequate sensitivity for resolving the NMR signal from bulk metal specimens in the presence of spurious transients produced by rf pulses.

C. Results on IN-100 Superalloy

Pulsed-inductive NMR experiments were performed on a powdered specimen of the superalloy IN-100.[17] The powder had particle sizes ranging from 105 to 177 μm. The principal elemental constituents of this alloy are nickel, cobalt, chromium, aluminum, and titanium; aluminum content is approximately 5% by weight. A sample amount of 22 g was used for the experiments reported here. The experiments were performed at ambient temperatures using conventional pulsed NMR equipment operating at a frequency of 10 MHz and a magnetic field of approximately 0.9T (9 kG).

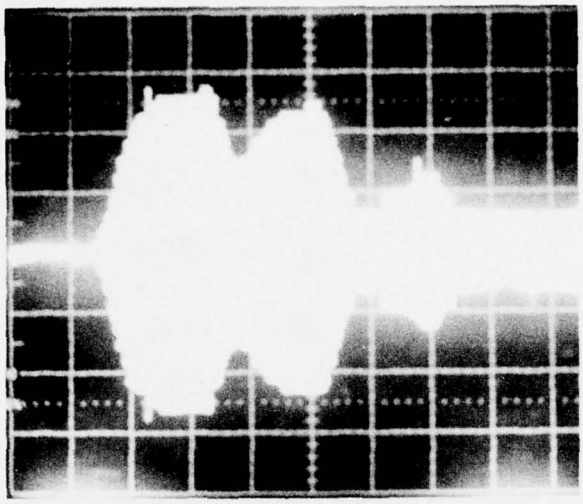

(a) Transient Response for 1/2-inch Diameter Aluminum Cylinder

1 V/div; 2 μs/div

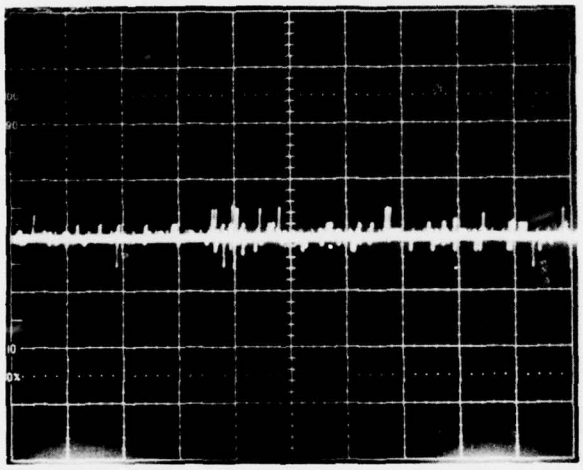

(b) Difference Signal for No Field Change

1 V/div; 2 μs/div

5008

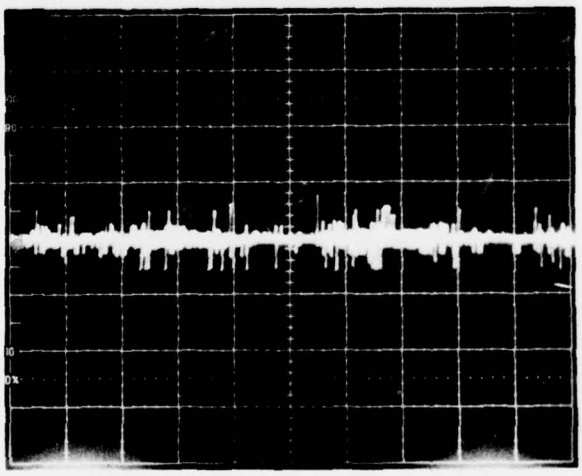

(c) Remnant NMR Signal-Difference Signal for 50 Gauss Field Change

1 V/div; 2 μs/div

FIGURE 11. ILLUSTRATION OF DIGITAL SUBTRACTION TECHNIQUE APPLIED TO A 1/2 IN.-DIAMETER ALUMINUM CYLINDER

Aluminum NMR signals were readily observed in the IN-100 specimen. In Figure 12a is shown a free-induction decay following a 90° pulse while a 90°-90° spin echo is shown in Figure 12b. Comparison with a specimen of pure aluminum indicates that signals from the aluminum in the IN-100 are reduced by a factor of approximately 25 from a comparable amount of pure aluminum. This reduction in signal amplitude may be caused by several factors, such as (1) incomplete penetration of rf fields through the particles due to skin effect, (2) cold-working associated with specimen preparation, (3) removal of signal contributions from nuclei subjected to quadrupolar interactions from neighboring atoms. The third factor is commonly observed in disordered dilute alloys and is the most likely cause of the large signal reduction.[18]

Although the NMR signals in IN-100 are rather weak, they can be enhanced for purposes of detailed investigation using signal averaging as shown by the FID presented in Figure 13. Analysis of the enhanced FID revealed a repeatable structure (identified by arrows in Figure 13) that is dependent on the magnetic field. This structure may be associated with an interfering NMR signal from vanadium (present at a level of approximately 1% by weight), which is only 0.1 MHz away from the ^{27}Al resonance.

The aluminum nuclear spin lattice relaxation times were determined by measuring signals displayed on an oscilloscope. Using a 90°-90° pulse sequence, the spin-spin relaxation time, T_2, was determind to be 230 ms, while the spin lattice relaxation time, T_1, was determined to be in the range of several ms. Both results are in agreement with results reported for dilute aluminum alloys.[19]

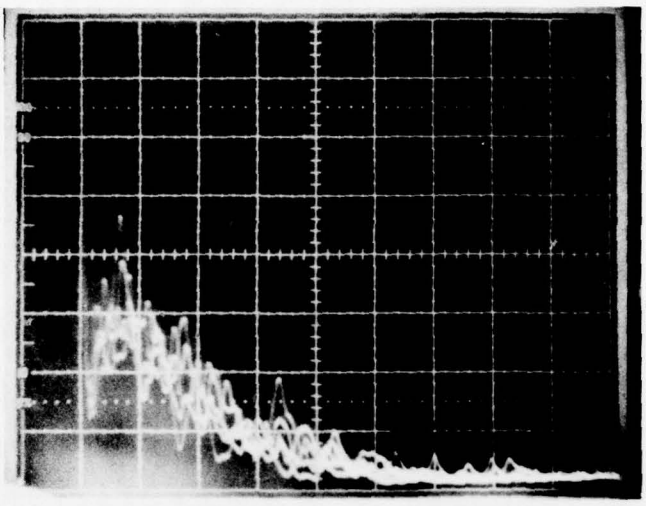

V = 0.1 V/div

H = 10 μsec/div

a. Free Induction Decay

5460

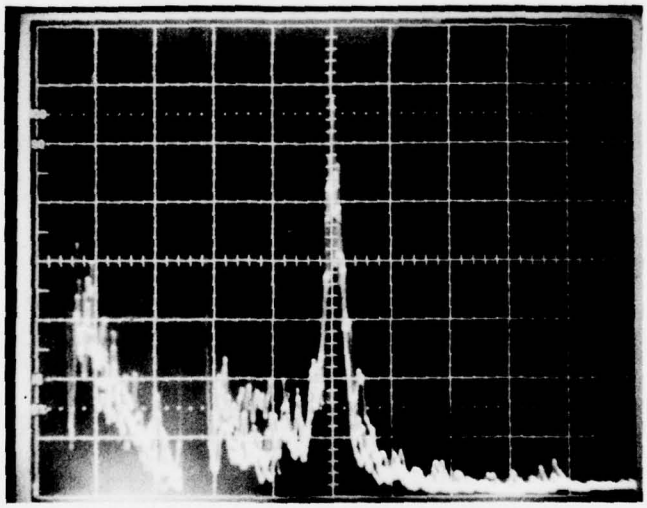

V = 0.1 V/div

H = 20 μsec/div

b. 90^{o} - 90^{o} Spin Echo

FIGURE 12. PULSED NMR SIGNALS FROM ALUMINUM IN THE IN 100 SUPERALLOY

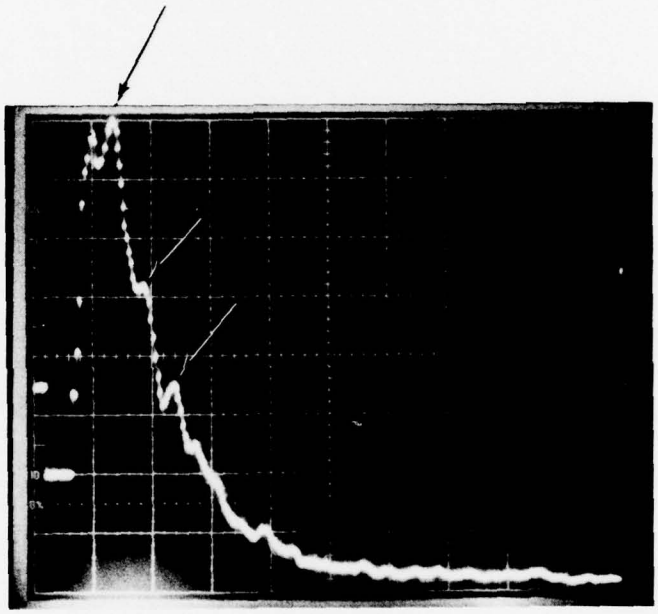

V = 0.5 V/div

H - 12.8 μsec/div

5461

FIGURE 13. SIGNAL AVERAGED FREE-INDUCTION-DECAY FROM ALUMINUM IN THE IN-100 SUPERALLOY

III. ACOUSTIC NMR

A. Specimens

Specimens for NAR were prepared from 99.999% pure polycrystalline aluminum purchased from the Materials Research Corporation as 1.91 cm (0.75 in.)-diameter rod. The rod stock was machined on a lathe to appropriate geometry and dimensions for the application of compressive and tensile deformation. For specimens to be deformed in compression, the rod stock was machined to lengths 5.08 cm (2 in.) long by 1.91 cm (0.75 in.) diameter, making sure that the end faces were flat and parallel to ensure homogeneous deformation. For the specimens deformed in tension, the rod stock was machined into standard tensile shape with a length of 13.34 cm (5.25 in.) and a gauge section diameter of 1.45 cm (0.57 in.). After machining, the specimens were stress-relieved at 600°C for three hours and allowed to air cool. The specimens were plastically deformed by compression or tension in various increments up to engineering strains of 25%. Since no previous results of the effect of strain on NAR in metals had been reported, the magnitude of the effect was unknown. For this reason, specimens were prepared with strains greater than expected in practical situations in order to enhance the probability of measureable effects. From each deformed specimen, two 1.27 cm (0.5 in.)-long by 1.27 cm (0.5 in.)-diameter cylinders were machined with the final passes being made very light to minimize surface damage. To provide a strain-free reference specimen, a 1.27 cm (0.5 in.)-long by 1.27 cm (0.5 in.)-diameter cylinder was machined from the same 1.91 cm (0.75 in.)-diameter aluminum rod stock used for the deformed specimens, and then annealed.

All of the cylindrical specimens were prepared for NAR by polishing the end faces flat and parallel. AC-cut transverse quartz transmitting and receiving ultrasonic transducers were bonded to the end faces of each specimen. The acoustics of the specimen were investigated by using an ultrasonic pulse-echo spectrometer, and also by examining the standing wave resonance pattern obtained while sweeping the frequency applied with an rf generator.

B. Experimental Approach

For the NAR experiments reported here a CW-transmission spectrometer, previously described in the literature, was used.[20] A block diagram of the arrangement is shown in Figure 14. In this system, a commercial signal generator (Hewlett Packard 608F) was used to provide the rf signal to the transmitting transducer. The rf signal at the receiving transducer was amplified and detected in a square law detector. The sensitivity of the system to small changes in acoustic attenuation was improved by modulation of the magnetic field and synchronous detection of the output. A time constant of 1 sec was used at the output of the synchronous detector to avoid distortion of the detected signals. Upon detection, the NAR signals were recorded on magnetic tape for later playback and analysis. For each specimen investigated, replicate runs were made in order to verify the repeatability of the measurements.

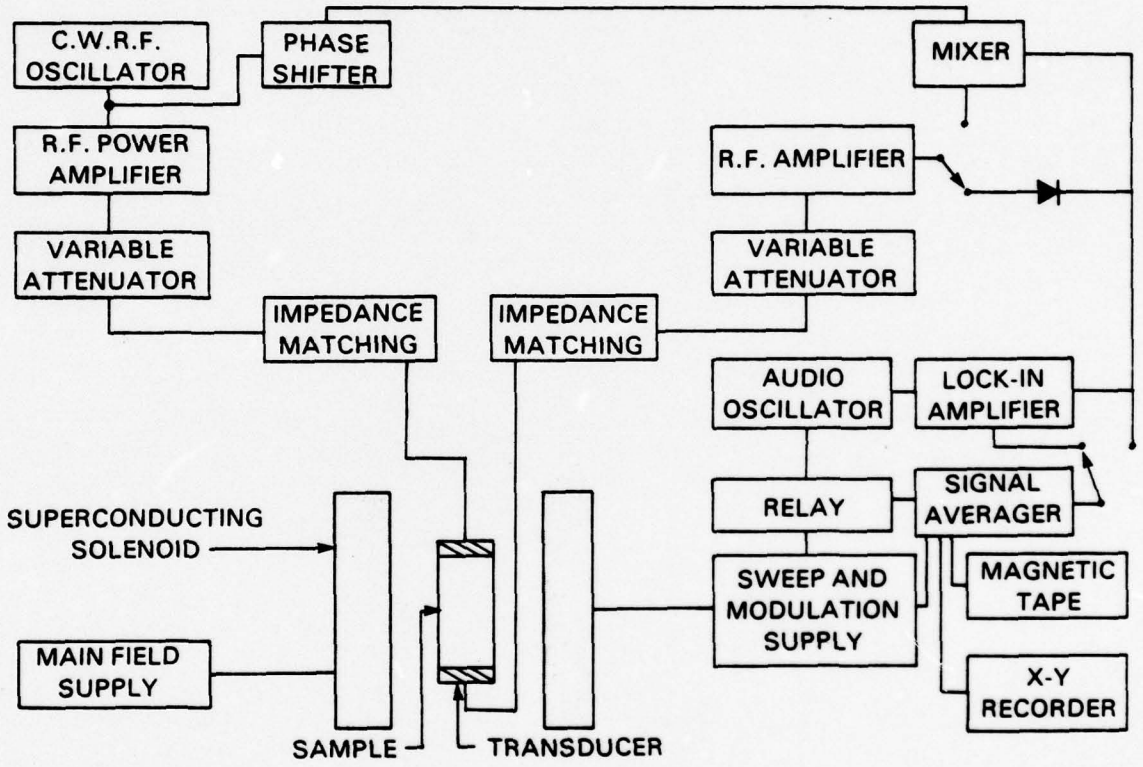

FIGURE 14. BLOCK DIAGRAM OF NUCLEAR ACOUSTIC RESONANCE APPROACH

The NAR experiments were performed at frequencies of approximately 60 MHz, and magnetic fields of approximately 5.4 T (54 kG). The frequency was held constant while the magnetic field was varied through the resonance value. Repetitive sweeps through resonance were made and the signal averaged to enhance the signal-to-noise ratio. In order to optimize the signal amplitude, most of the experiments were conducted at a temperature of 4.2°K.; however, NAR signals from the unstrained specimen could not be observed at this temperature, and therefore a higher temperature of 65°K was used. Although it is not clear at this time why NAR could not be observed at 4.2°K in the unstrained aluminum specimen, it may be related to the anomalous temperature dependence of NAR reported for a pure single crystal of aluminum.[21] This result for single crystal aluminum has been interpreted in terms of attenuation and phase shift associated with the modulation field inside the metal sample.[22]

C. Results on Plastically Deformed Aluminum Specimens

Typical NAR signals obtained from aluminum specimens subjected to various amounts of compressive deformation are shown in Figure 15. The indicated engineering strain values were determined by measuring the changes in specimen length due to deformation with a micrometer. The displayed NAR signals are the first derivatives of the acoustic absorption. The amplitudes of these signals cannot be directly compared since this parameter is affected by the bonding characteristics of the transducers, among other factors. However, all of the detected NAR signals were found to be asymmetric in agreement with previously reported results for single crystal aluminum.[11] This asymmetry has been shown both experimentally[23] and theoretically[24] to be associated with an admixture of χ' and χ'' (the real and imaginary parts, respectively, of the complex nuclear susceptibility) according to the following expression for the resonant acoustic absorption

$$\Delta\alpha \propto [(1-\beta^2)\ \chi''- 2\beta\chi'] \qquad (1)$$

where β is equal to $\omega c^2/4\pi\sigma_0 v^2$, where c is the velocity of light, σ_0 is the electrical conductivity and v is the acoustic velocity. The admixing of χ' and χ'' to produce an asymmetric first derivative signal is illustrated schematically in Figure 16.

1. Linewidth vs. Strain

The NAR signals from deformed aluminum were analyzed to obtain information on the acoustic absorption linewidth. The linewidths were determined by measuring the peak-to-peak separations of the experimentally recorded first derivative signals. Results are presented in Table I. The first derivative linewidth for the unstrained polycrystalline specimen compares favorably to the result reported for single crystal aluminum.[11] According to the theory proposed by Kanert for the influence of strain on NMR,[25] the linewidth should increase with increasing strain, and at a high value of strain the width should decrease again (see Appendix). Examination of Table I indicates that this linewidth behavior was observed for the tension specimens; however the strain dependence of the linewidth for the compression specimens is not clear.

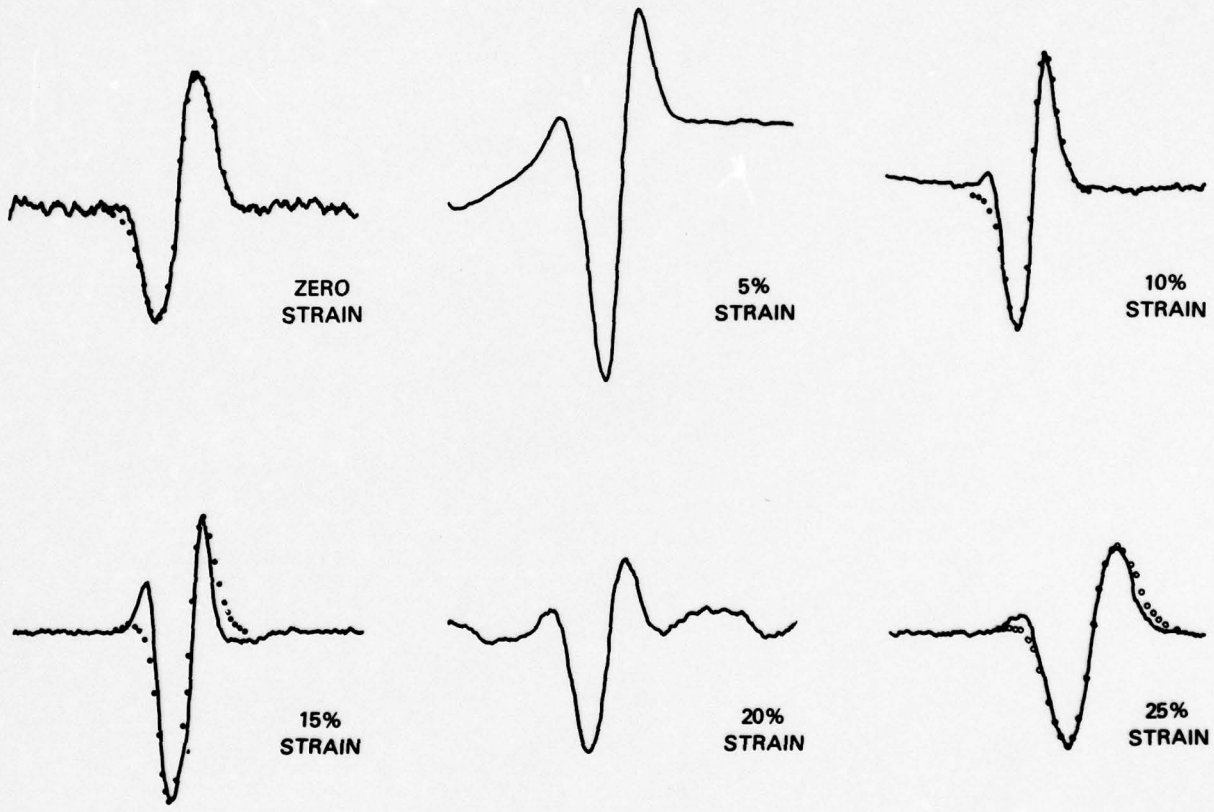

5553

FIGURE 15. DEPENDENCE OF ALUMINUM ACOUSTIC ABSORPTION FIRST DERIVATIVE ON COMPRESSIVE STRAIN

Open Circles Represent the Gaussian Lineshape;
The Solid Line Shows the Experimental NAR signals

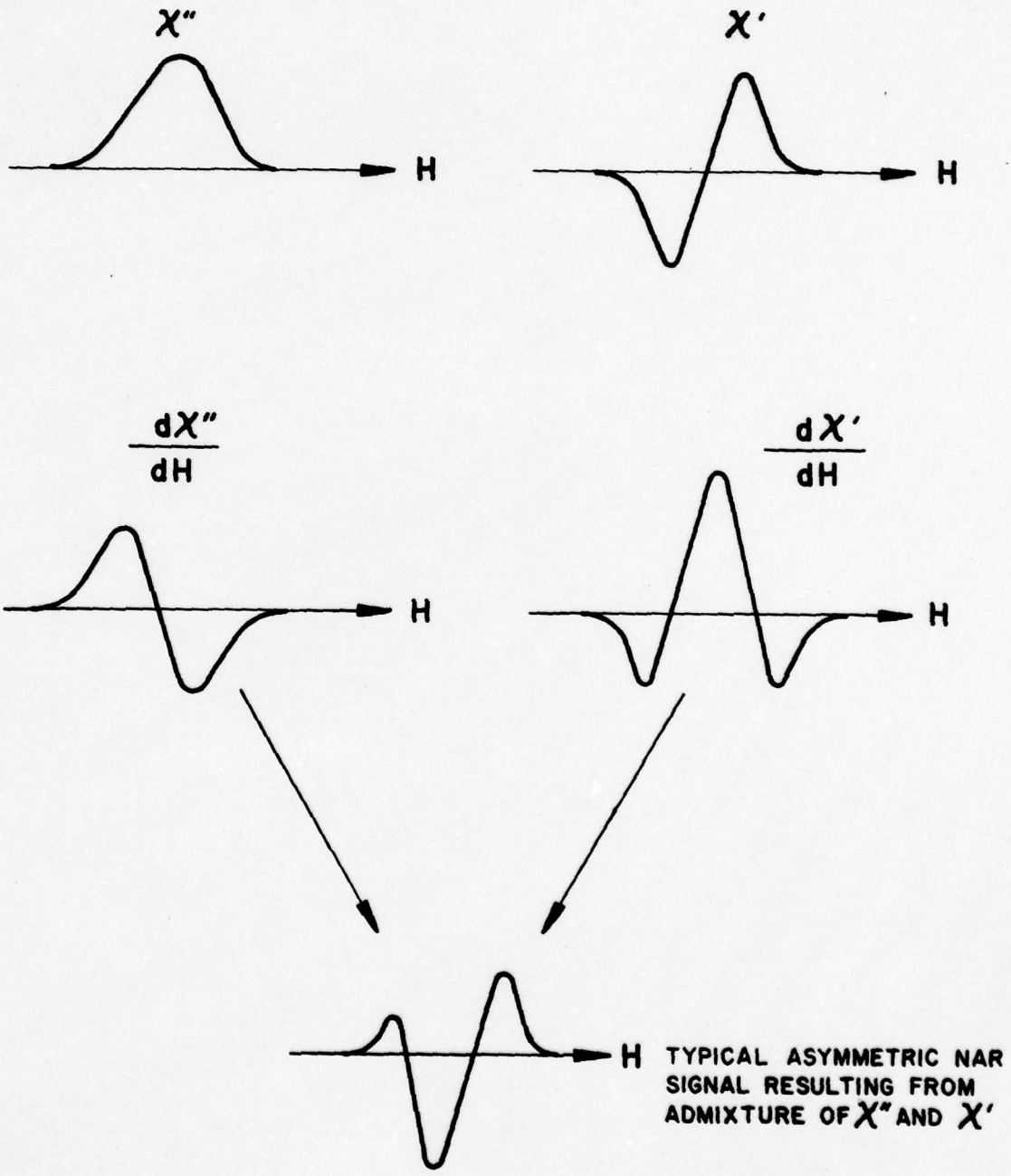

5554

FIGURE 16. SCHEMATIC REPRESENTATION OF ADMIXTURE OF χ' AND χ"

TABLE I

Experimental NAR First Derivative Linewidth in Aluminum Vs. Residual Strain

Compression			Tension		
Specimen No.	Strain (%)	Linewidth (G)	Specimen No.	Strain (%)	Linewidth (G)
U	0	7.0	U	0	7.0
C5	5	8.0	T5	5	8.5
C10	10	7.3	T10	10	8.9
C15	15	7.2	T15	15	10.9
C20	20	8.9	*	--	--
C25	25	8.0	T25	25	5.6

* A 20% tensile deformation specimen was not prepared.

Different linewidth behavior may be observed for the tension and compression specimens since the quadrupolar distortion depends on the density and types of dislocations which may be different for the two modes of deformation.

2. Lineshape vs. Strain

The experimental NAR lineshapes were analyzed to determine the relative percentages of χ' and χ''. This was done by first measuring the relative amplitudes of the peaks of the asymmetric NAR signals. This information was used to compute Gaussian lineshapes for comparison with the experimental curves. The χ'' percentages obtained in this way are listed in Table II. These results show that the NAR lineshape changes monotonically with deformation. The percentage of χ'' decreases from 88% for the unstrained sample to 55% for specimen C25 and 70% for specimen T25.

As mentioned earlier, the acoustic absorption lineshape depends on the admixture of χ' and χ'' through the factor β, which in turn is dependent on the conductivity and acoustic velocity. Since the changes in acoustic velocity with strain are too small to produce the experimentally observed admixture of χ' and χ'', an analysis was performed on the possibility that the lineshape changes were produced by changes in the conductivity with strain. For the undeformed samples an 88% χ'' lineshape corresponds to a β of 0.05. This is also the value of β computed using the published conductivity for unstrained high purity aluminum at 60°K[26] and known sound velocity. Thus, the lineshape for undeformed polycrystalline aluminum is in agreement with that predicted from Equation (1).

For analyzing the effect of deformation on lineshape, the results for specimen T25 were used. For this case, the experimentally observed lineshape (70% χ'') corresponds to approximately $\beta = 0.16$, which implies a resistivity change due to deformation of 0.2 $\mu\Omega$-cm. Experimentally, the increase in resistivity $\Delta\rho$ is found to be a linear function of deformation[27]

$$\Delta\rho = A\varepsilon \tag{2}$$

The directly measured value of A varies considerably for aluminum. Presumably, the value of A is affected by the purity of the metal and the strain condition before deformation. According to Cohn[27], A = 0.021 $\mu\Omega$-cm for 99.997% pure aluminum deformed at 77°K, and A = 0.166 $\mu\Omega$-cm for 99.986% pure aluminum deformed at 77°K.

Using an A value of 0.020 $\mu\Omega$-cm (since the aluminum used for the NAR experiments was 99.999% pure), the resistivity change for 25% deformation is computed from Equation (2) to be

$$\Delta\rho = (0.020\ \mu\Omega\text{-cm})\ (.25) = 0.005\ \mu\Omega\text{-cm} \tag{3}$$

This resistivity change is more than an order of magnitude less than the value of 0.2 $\mu\Omega$-cm implied by the NAR lineshape changes. Even the resistivity change computed for the less pure aluminum (99.986%) is over five

TABLE II

The Imaginary Component, χ'', of the Complex Nuclear Susceptibility from NAR in Plastically Deformed Aluminum

Compression			Tension		
Specimen No.	Strain (%)	χ'' (%)	Specimen No.	Strain (%)	χ'' (%)
U	0	88	U	0	88
C5	5	75	T5	5	87
C10	10	78	T10	10	85
C15	15	63	T15	15	74
C20	20	60	*	--	--
C25	25	55	T25	25	70

* A 20% tensile deformation specimen was not prepared.

times less than the NAR implied value. These results imply that the experimentally observed NAR lineshape changes with deformation cannot be explained solely by resistivity changes and that other factors must be taken into account such as the influence of quadrupolar distortions produced by strain.

Analysis of the experimental NAR lineshapes in terms of a Gaussian function indicated that the lineshape for the undeformed specimen agreed reasonably well with a Gaussian function while the lineshapes for the more highly deformed samples deviated from a Gaussian function. This is illustrated in Figure 15 where the computed Gaussian lineshapes are represented as open circles (the baselines of the experimental curves for specimens C5 and C20 were not well enough defined to allow computation of a Gaussian lineshape). Examination of Kanert's theory indicates that deviation from a Gaussian lineshape is predicted at higher strains.[25] The theoretical NMR absorption signal as a function of strain is given by Kanert as (see Appendix)

$$g(y,Z) = ae^{-y^2/2} + bZ^2 \int_{-\infty}^{\infty} \frac{e^{-x^2/2}}{Z^3 + |y - x|^3}\, dx \qquad (4)$$

where y is the magnetic field variable, Z is the normalized quadrupolar distortion due to lattice strain and a and b are constants. Note that the lineshape g(y,Z) is the sum of a Gaussian function (first term) and the second term which depends on lattice strain. This equation was numerically evaluated for two different values of Z. These results are shown in Figure 17 compared with Gaussian functions fitted to the peak of the function g(y,Z). As is seen in Figure 17 the function g(z,Z) increasingly deviates from a Gaussian for greater Z. Thus, the experimentally observed deviation from a Gaussian function for the NAR signals obtained from highly deformed specimens is in qualitative agreement with Kanert's theory.

3. Separation of Experimentally Observed NAR Signals into χ' and χ'' Components

As mentioned earlier, the lineshape recorded in an NAR experiment is a mixture of the real and imaginary parts of the nuclear susceptibility, χ' and χ''. For comparison with theory, it is desireable to separate the experimentally observed signals into these components. Since the functional form of the lineshapes for the deformed specimens is not known (it was shown in the previous section that these lineshapes are not Gaussian), the separation must be done numerically without assuming any particular lineshape function. To do this, a method developed by Sagalyn and Hoffman[28] for induction NMR signals was modified for application to NAR. Sagalyn and Hoffman utilized their approach for separating the NMR signals from bulk metal specimens where the sample dimension is much greater than the rf skin depth into absorption and dispersion components. The modification of this method for application to NAR is as follows:

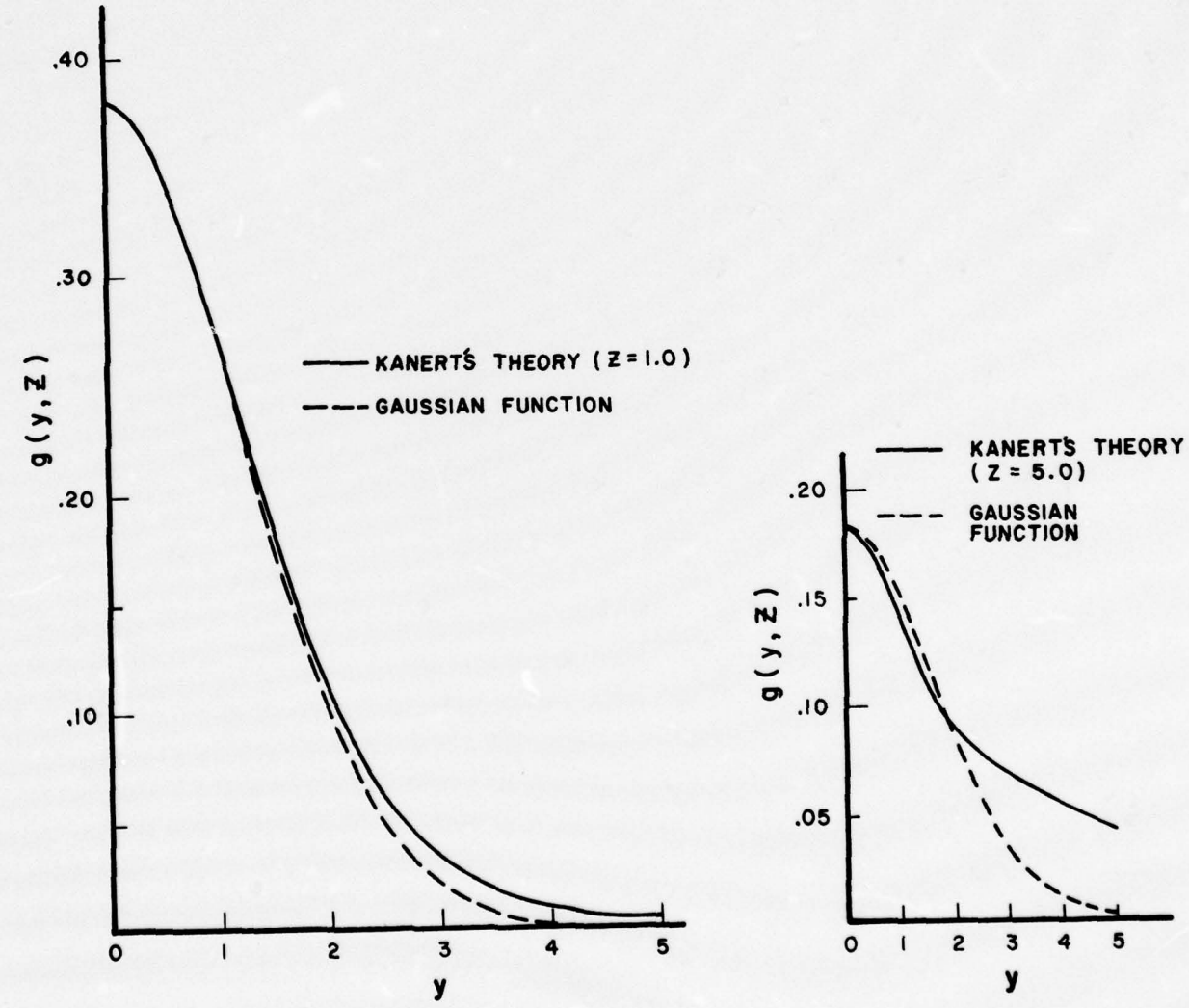

5555

FIGURE 17. COMPARISON OF THEORETICAL STRAIN-BROADENED LINESHAPE WITH GAUSSIAN FUNCTION

Let $f(\nu)$ be the experimental lineshape

$$f(\nu) = a \frac{d\chi'(\nu)}{d\nu} + b \frac{d\chi''(\nu)}{d\nu} \tag{5}$$

Define

$$g(\nu) = a\chi' + b\chi'' \tag{6}$$

Then

$$g(\nu) = \int_o^{\nu} f(\nu')d\nu' \tag{7}$$

is just the integral of the experimental lineshape. Further define

$$h(\nu) = a\chi' - b\chi'' \tag{8}$$

and use the Kramers Kronig relation[29]

$$h(\nu) = \frac{a}{\pi} \int_o^{\infty} \frac{d\chi''(\nu')}{d\nu'} \ell n \left|\frac{\nu o}{\nu' - \nu}\right| d\nu' + \frac{b}{\pi} \int_o^{\infty} \frac{d\chi'(\nu')}{d\nu'} \ell n \left|\frac{\nu o}{\nu' - \nu}\right| d\nu' \tag{9}$$

After simplification

$$h(\nu) = -\frac{1}{\pi} \int_o^{\infty} f(\nu') \ell n|\nu' - \nu| d\nu' \tag{10}$$

Then

$$\chi'(\nu) = \frac{1}{2a}\left[g(\nu) + h(\nu)\right] \tag{11a}$$

$$\chi''(\nu) = \frac{1}{2b}\left[g(\nu) - h(\nu)\right] \tag{11b}$$

To remove the logarithmic singularity in Equation 10, $h(\nu)$ can be transformed to

$$h(\nu) = -\frac{1}{\pi} \int_{-\infty}^{\infty} \left[f(\nu - e^x) + f(\nu + e^x)\right] xe^x dx \tag{12}$$

Computer programs were developed to numerically integrate the experimental NAR signals to obtain the functions $g(\nu)$ and $h(\nu)$. These functions could then be used to obtain the χ' and χ'' components according to Equations 11a and 11b. Typical results obtained are shown in Figure 18.

Although the procedure above was shown to be useful for separating the experimental NAR signals into χ' and χ'' components without resorting to assumptions regarding the functional form of the lineshape, difficulties were encountered in that the resultant χ'' was quite sensitive to the baseline choice for the experimental signals. Although the experimental NAR signal-

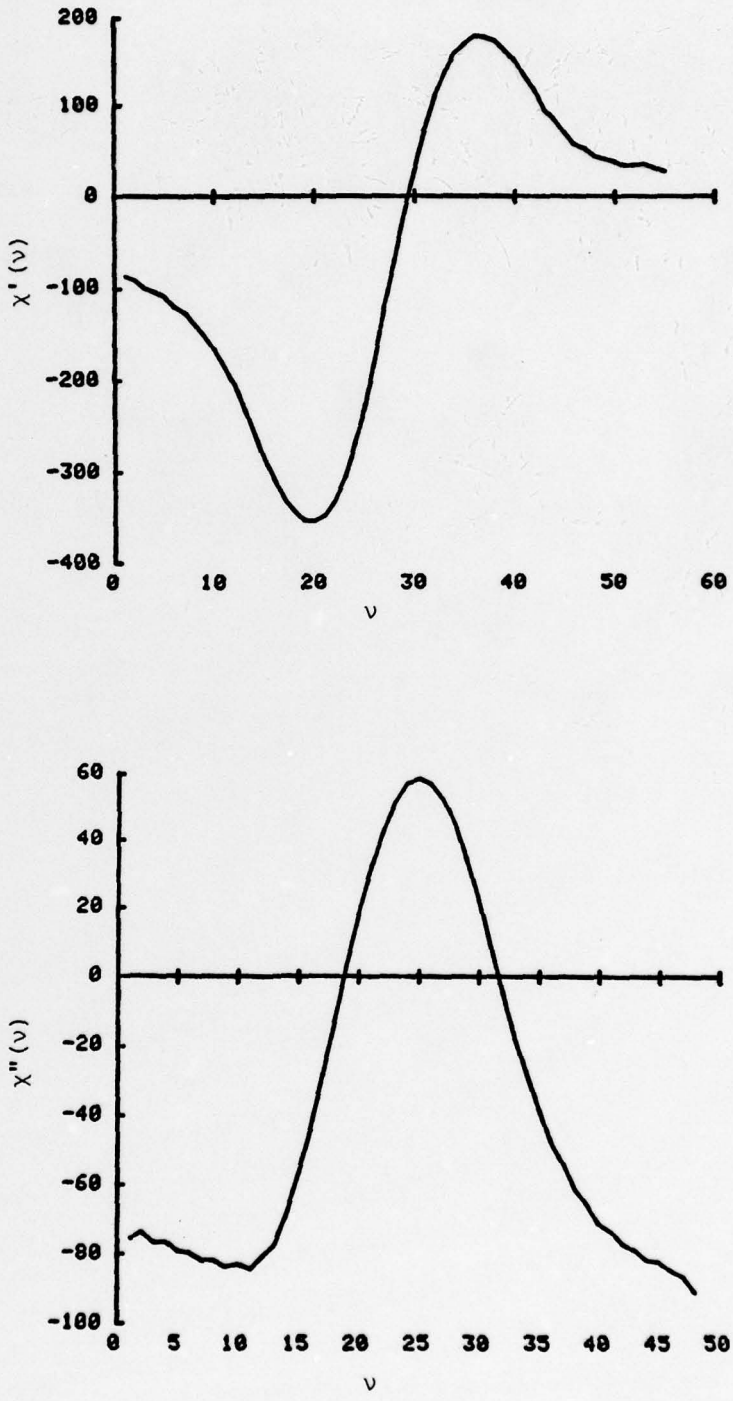

5556

FIGURE 18. COMPUTER EXTRACTED χ' AND χ'' COMPONENTS FROM EXPERIMENTAL NAR SIGNALS FOR 5% TENSILE STRAINED ALUMINUM

to-noise ratio was reasonably good, in some cases the baseline was difficult to precisely determine, resulting in distortion of the computer-extracted χ'' components.

4. Modulation Effects

Results were obtained indicating that the acoustic absorption lineshape for the deformed aluminum specimens is dependent on the frequency and amplitude of the magnetic field modulation. The experiments conducted show that for a relatively lightly deformed specimen (0 to 5% strain) the NAR lineshape is essentially independent of modulation frequency (results were obtained in the 25 to 100 Hz range), whereas for a highly deformed specimen (25% strain), the lineshape changes substantially with modulation frequency. These results are illustrated in Figure 19. In fact, as the modulation frequency decreases from 100 Hz to 35 Hz the linshape for specimen T25 changes from approximately 50 or 60% χ'' to approximately 20% χ''.

Further exploration of modulation effects showed that specimen T25 exhibited a shift in position of the resonance signal with variation in modulation amplitude. For a change in modulation amplitude from 1 mT (10 G) to 2 mT (20 G) the position of the NAR signal for specimen T25 varied by approximately 1.6 mT (16 G). Investigation of this modulation effect on the undeformed specimen and specimen T5 indicated that there was no shift of the resonance position with changes in modulation amplitude for these specimens.

Although no explanation can be advanced for the shift of the NAR signal with modulation amplitude, the changes with modulation frequency may be explained in terms of penetration depth. Since the modulation frequency determines the depth of penetration of the magnetic field into the specimen, a possible interpretation of these results is that the change in lineshape observed for specimen T25 may be associated with inhomogeneous deformation existing in the specimen. An important practical implication of this result is that potentially NAR may be used to probe different regions of a specimen by varying the modulation frequency. The resulting NAR signal shape would give information on the stress conditions prevailing in the regions probed. Thus, by properly varying the modulation frequency, a profile of the internal stress field within the specimen might be obtained.

D. Additional Results

1. Aluminum Copper Alloys

To investigate the applicability of NAR to polycrystalline aluminum alloys, experiments were performed on specimens containing 1.4% and 2.8% copper by atomic weight. After preparation and thermal homogenization the alloys in the form of 1.9 cm (0.75 in.)-diameter rods were machined to cylinders 1.27 cm (0.5 in.) diameter by 1.27 cm (0.5 in.) long, with the final passes being made very light to minimize surface damage. The specimens were prepared for NAR as described previously. NAR data were obtained at a frequency of approximately 60 MHz and a temperature of 4.2°K. Signal averaging was used to enhance the signal-to-noise ratio.

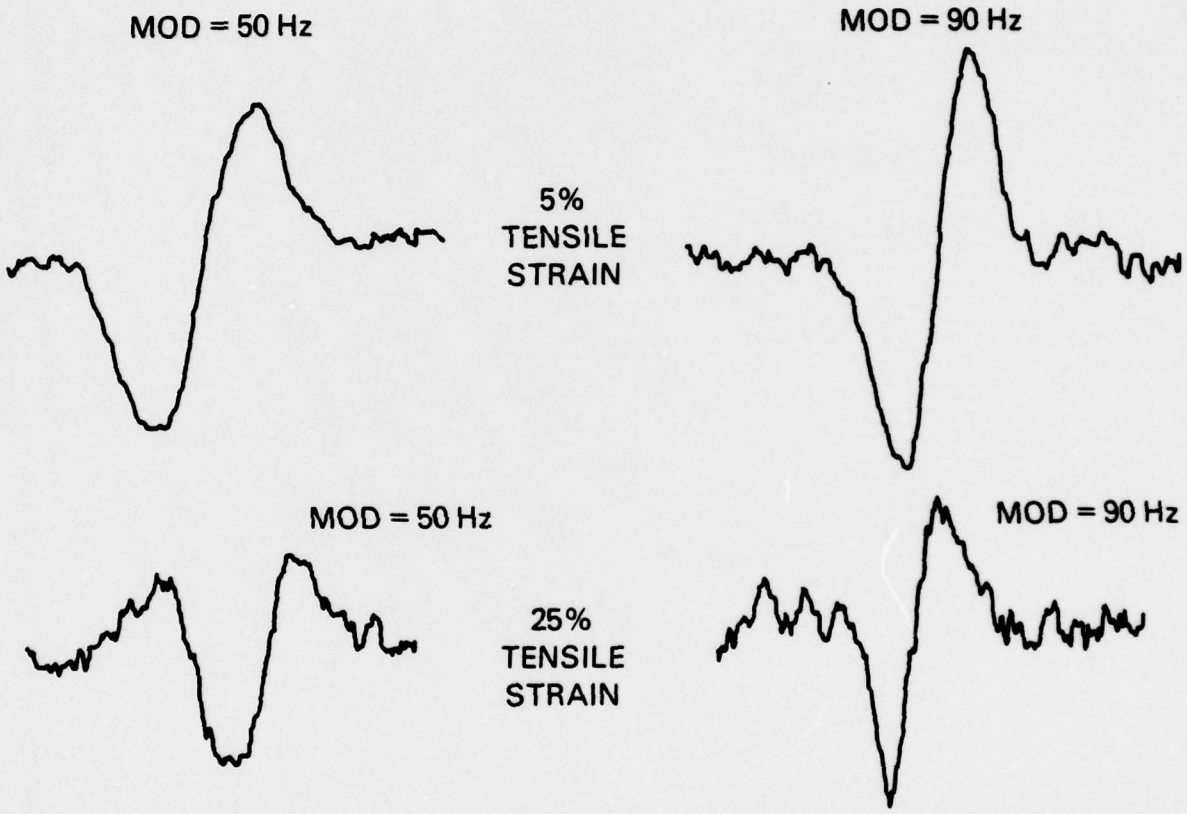

FIGURE 19. EFFECT OF MODULATION FREQUENCY ON NAR LINESHAPE AS A FUNCTION OF PLASTIC DEFORMATION IN POLYCRYSTALLINE ALUMINUM

The recorded NAR first derivatives of the acoustic absorption obtained from the two aluminum alloys are shown in Figure 20. A high modulation level was used in order to obtain good signal-to-noise ratio with the result that the linewidths given in the Figure are modulation broadened values. As in the case of pure polycrystalline aluminum, the acoustic absorption line shapes are asymmetric. This asymmetry may be interpreted in terms of the decrease in electrical conductivity due to the addition of copper. The measured asymmetry can be accounted for by assuming a conductivity at $4.2^{\circ}K$ of 1.5×10^{6} $(\Omega\text{-cm})^{-1}$, which is a reasonable value for these alloys.[30]

2. NAR Using Electromagnetic Acoustic Generation

Limited experiments were performed to determine the feasibility of using electromagnetic acoustic transducers (EMATs) for the generation and detection of NAR. Electromagnetic generation has been under development for about ten years for ultrasonic nondestructive examination and several practical applications utilizing this approach have been reported.[31] The primary advantage of EMATs for nondestructive evaluation is that it is not necessary to bond transducers to the material of interest. This noncontacting feature enables ultrasonic inspection to be utilized in situations where bonding of transducers is not feasible, e.g., under high temperature and for rapid scanning.

An EMAT coil was constructed consisting of 27 turns of No. 28 copper wire wound on a Plexiglass form. The coil was on an end face of one of the cylindrical aluminum specimens which was in the gap of an electromagnet, as shown in Figure 21. The EMAT coil and the specimen were oriented so that the external dc magnetic field was directed in the plane of the end surface of the sample and perpendicular to the copper wire windings of the EMAT coil. With this orientation, longitudinal ultrasonic waves were produced in the specimen with the ion motion directed along the axis of the specimen cylinder. An X-cut transducer was bonded to the second face of the specimen to act as a receiver for the standing waves set up by the EMAT coil. Figure 22 shows the acoustic mechanical resonance standing wave pattern for specimen T5 generated with the EMAT and detected with the X-cut transducer at a frequency of 10 MHz and a magnetic field of 0.895 T (8.95 kG). Although the pattern indicates that the standing wave mode structure is complicated, the resonance peaks are reasonably sharp and the separation of approximately 0.25 MHz is comparable to that observed for standing waves set up by a bonded transducer. Attempts to observe NAR signals were unsuccessful; however, this may be attributed to the low frequency and high temperature conditions for these experiments. In addition, the complex standing wave pattern produced by the EMAT served to reduce the intensity for NAR detection. It appears, however, that with additional developmental effort suitable standing wave patterns with sufficient intensity could be set up for NAR detection using EMATs. Successful development of this approach would greatly enhance the applicability of NAR for nondestructive evaluation.

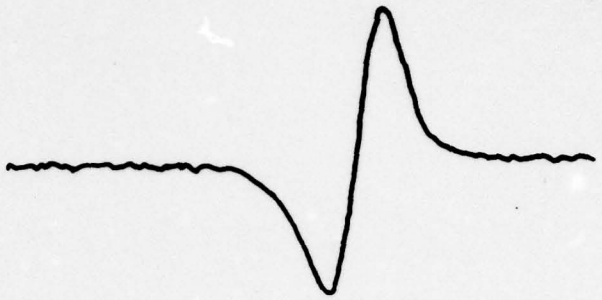

Al - 1.4 % Cu
LINEWIDTH = 12.5 GAUSS

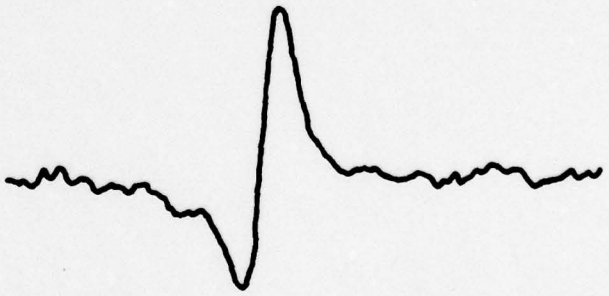

Al - 2.8 % Cu
LINEWIDTH = 12.4 GAUSS

FIGURE 20. ^{27}Al ACOUSTIC NMR SIGNALS FROM TWO Al-Cu ALLOYS

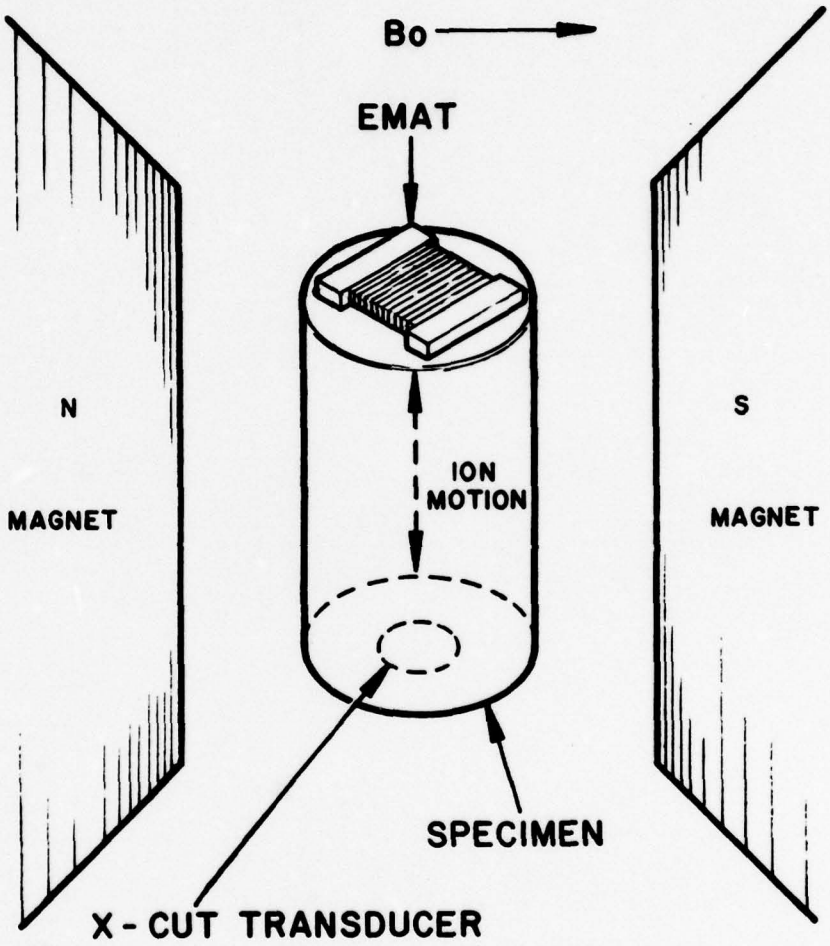

5558

FIGURE 21. SCHEMATIC ILLUSTRATION OF ELECTROMAGNETIC GENERATION OF LONGITUDINAL ACOUSTIC STANDING WAVES IN ALUMINUM CYLINDER

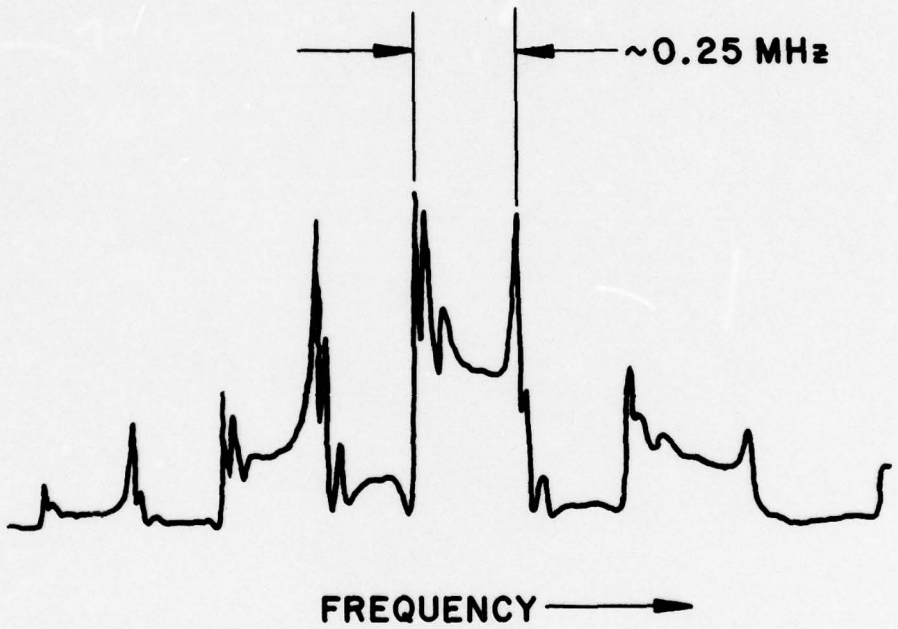

5559

FIGURE 22. ULTRASONIC STANDING WAVE SPECTRUM GENERATED IN AN ALUMINUM CYLINDER BY EMAT IN FREQUENCY RANGE OF 9 MHz to 11 MHz

IV. DISCUSSION

The aluminum NAR results presented in Section III are the first report of NAR signals from a polycrystalline metal. Previously, NAR in metals had been studied exclusively in single crystal specimens. The primary reason for using single crystals in previous research was to obtain fundamental information on the orientation dependence of NAR signals. Thus, prior to this project, the feasibility of detecting NAR signals in polycrystalline metals had not been established. A potential problem was that there could possibly be too much absorption and scattering of the ultrasonic standing waves making NAR signals undetectable. It was found, however, that NAR was readily observed from polycrystalline aluminum and the signals were comparable in amplitude and lineshape to those previously reported for single crystal aluminum. Also, the NAR signals in polycrystalline aluminum are asymmetric due to an admixture of χ' and χ'' with the relative percentages in agreement with results reported for single crystal aluminum.

The NAR results obtained for plastically deformed aluminum are in qualitative agreement with Kanert's theory of strain-induced quadrupolar interactions with the exception of the NAR linewidth variation for aluminum specimens deformed in compression for which comparison with theory is inconclusive. Although Kanert's theory was developed for the effect of lattice strain on inductive NMR, the fact that it explains the experimental NAR results means that the same fundamental mechanisms responsible for the variations in NMR signals, namely, electric quadrupole interactions, are also responsible for the observed NAR lineshape changes. It thus appears that with suitable modification, Kanert's theory can be expanded to include the effect of quadrupole perturbations on the χ' component as well as χ'' so that the theoretical admixture of χ' and χ'' due to strain-induced quadrupole interactions may be determined. Availability of such a modified theory would enable the experimental NAR lineshapes to be quantitatively interpreted in terms of the sense and degree of deformation. Experimental verification of Kanert's theory modified for NAR might be obtained by performing NAR experiments on specimens which were characterized metallurgically with respect to dislocation type and density both before and after deformation.

For the deformed aluminum specimens, the NAR lineshape was found to vary with modulation frequency; the magnitude of the effect depends on the amount of plastic deformation. As indicated in the previous section, an important consequence of the dependence of NAR lineshape on modulation is the potential for measuring internal distributions of stress and strain. To further explore the relationship between lineshape and modulation, experiments should be performed utilizing specimens with controlled deformation gradients. By varying the modulation frequency, the penetration depth could be changed thereby providing a basis for relating the NAR lineshape to a known stress gradient. These results could then be compared with NAR lineshapes obtained from uniformly deformed specimens.

The NAR experiments reported in Section III were performed in a superconducting magnet at a field of approximately 5.4 T (54 kG) with specimen temperatures varying from 4.2°K to approximately 60°K. These conditions were chosen based on available NAR apparatus. However, NAR

signals in aluminum have been reported at room temperature and a magnetic field of 2 T (20 kG).[11] Thus for practical application of NAR to residual stress measurement, it should be possible to use lower magnetic fields and higher temperatures. Although the NAR response decreases with decreasing magnetic field and increasing temperature, signal averaging should provide sufficient enhancement of the signal to enable a lineshape measurement to be made.

Although pulsed inductive NMR signals from aluminum cylinders were masked by the acoustic transient response, NMR results obtained on IN-100 powder were very encouraging. Initially, it was thought that the small amount of aluminum in this alloy and the complicated nature of the system would render the aluminum signal difficult to observe. However, aluminum NMR signals were readily observed using pulsed NMR techniques. One implication of these results is that IN-100 is amenable to study using NMR to provide detailed information about the internal magnetic and electronic structure of this important material. Such information would be very useful to metallurgists and material scientists in better understanding the nature of this nickel-base superalloy and in providing guidance for developing improved materials. A further implication of these preliminary results concerns nondestructive inspection of components fabricated from IN-100, in particular, the measurement of residual stress. Considering the critical application of superalloys in jet engine components, the development of an NDE method for residual stress measurement would be of great importance.

V. CONCLUSIONS AND RECOMMENDATIONS

From an analysis of the results obtained in this research, the following conclusions were reached:

1. The influence of plastic deformation on experimentally observed NAR signals in polycrystalline aluminum is in qualitative agreement with present NMR theory.

2. Analysis of the NAR lineshape can provide information on the sense and degree of deformation.

3. The dependence of the NAR lineshape on modulation frequency could provide a means for determining internal stress distributions.

4. Magnetic resonance techniques are applicable to NMR nuclei in superalloys as evidenced by the observation of of pulsed NMR signals from the aluminum constituent in the nickel-base superalloy IN-100.

Based on results of the research, the following recommendations are made:

1. Modify Kanert's theory for the effect of deformation on NMR to include the effect of deformation on NAR lineshapes.

2. Perform NAR experiments on metallurgically well-characterized specimens which have been plastically deformed to enable quantitative comparison with theory.

3. Investigate the application of NAR to superalloys, such as IN-100, as the basis for nondestructive measurement of residual stress.

VI. SUPPLEMENTARY INFORMATION

A. Publications

The program background and initial results were presented in "Nuclear Resonance for the Nondestructive Evaluation of Structural Materials", G. A. Matzkanin, Proceedings of the ARPA/AFML Review of Progress in Quantitative NDE, Technical Report AFML-TR-77-44, pp. 78-83, September 1977.

The NAR results obtained on the deformed aluminum specimen are discussed in "Investigation of Nuclear Acoustic Resonance for the Nondestructive Determination of Residual Stress", G. A. Matzkanin, R. G. Leisure and D. K. Hsu, presented at the ARPA/AF Review of Progress in Quantitative NDE, July 8-13, 1979, La Jolla, California. Proceedings in print.

A publication co-authored by G. A. Matzkanin and D. K. Hsu documenting all of the NAR results discussed in this Final Report is planned for submission to a refereed technical journal in the Spring of 1980.

B. Personnel

The Principal Investigator of this program was Dr. George A. Matzkanin, Sr. Research Physicist, in the Instrumentation Research Division at Southwest Research Institute. Much of the experimental inductive NMR work was performed by E. S. Riewerts, Engineering Technologist, in the Instrumentation Research Division. Serving as consultant on the NAR study during the first two years of the program was Prof. Robert G. Leisure, Department of Physics, Colorado State University. The NAR measurements during this time were performed by Graduate Assistant, Mr. Donald Allred, under the supervision of Prof. Leisure. Prof. David K. Hsu, Department of Physics, Colorado State University, served as consultant on the NAR aspects of the program during the third year and supervised experiments performed by Graduate Assistant, Mr. Gary Ashton.

C. Coupling

Throughout the course of the program, coupling was maintained between Southwest Research Institute and Colorado State University. In addition, during the summer of 1979, Prof. Hsu took part in an NSF-funded Industrial Research Participation Program for Science Faculty. Dr. Hsu's efforts on the NAR aspects of the AFOSR program formed the basis for his work as an industrial research participant. The experience he gained is expected to be extremely valuable in initiating graduate and under graduate academic programs in NDE-related areas.

VII. REFERENCES

1. Proceedings of a Workshop on Nondestructive Evaluation of Residual Stress, NTIAC-76-2, August, 1975.

2. Cook, T. S., Lankford, J., and Sheldon, G. P., "Research on Growth of Microcracks in Nickel-Base Superalloys", AFML-TR-78-133, September, 1978.

3. Marion, R. H., "Anomalies in Measurement of Residual Stress by X-Ray Diffraction", Proc. of a Workshop on NDE of Residual Stress, NTIAC-76-2, August 1975, pp. 127-135.

4. Barton, J. R. and Kusenberger, F. N., "Residual Stresses in Gas Turbine Engine Components from Barkhausen Noise Analysis", J. for Engineering and Power, October 1974, pp. 349-357.

5. Tokuoka, T. and Iwashimizur, Y., "Acoustical Birefringence of Ultrasonic Waves in Deformed Isotropic Elastic Materials", Int. J. Solids Structures 4, 383(1968), and references cited therein.

6. Baer, W. H., Yagnik, C. M., and Collins, R. L., "Residual Surface Stress in Ferrous Metals by Mossbauer Spectroscopy", Proc. of 10th Symposium on Nondestructive Evaluation, San Antonio, Texas, April, 1975, pp. 194-208.

7. Marion, R. H. and Cohen, J. B., Advances in X-Ray Analysis, Vol. 18, Plenum Press, New York, 1974, pp. 466-501.

8. Saterlie, S., Johnson, M. L., Alexopoulos, P., Seppi. F., Ure, R., and Byrne, J. G., "Positron Annihilation Observations of Shot Peened Aluminum Alloys", Phys. Stat. Sol. (a)41, K75 (1977).

9. Gardner, C. G., "NDE of Residual Stress: An Overview", Proc. of a Workshop on Nondestructive Evaluation of Residual Stress, August 13-14, 1975, San Antonio, Texas, pp. 1-9.

10. Matzkanin, G. A., "Nuclear Resonance for the Nondestructive Evaluation of Structural Materials", AFML-TR-77-44, pp. 78-84, September, 1977.

11. Buttet, J., Gregory, E. H., and Baily, P. K., "Nuclear Acoustic Resonance in Aluminum Via Coupling to the Magnetic Dipole Moment", Phy. Rev. Lett. 23, 1030 (1969).

12. Andrew, E. R., Nuclear Magnetic Resonance, Cambridge University Press, Cambridge, England, 1955.

13. Slichter, C. P., Principles of Magnetic Resonance, Harper Row, New York, 1963.

14. Poole, C. P., Jr., and Farach, H. A., Relaxation in Magnetic Resonance, Academic Press, New York and London, 1971.

15. Weisman, I. D., Swartzendruber, L. J., and Bennett, L. H., "Nuclear Resonances in Metals: Nuclear Magnetic Resonance and Mossbauer Effect", in Metals Progress, Vol. 6, Pt. 2, John Wiley & Sons, Inc., 1973, pp. 490-496.

16. Pacult, Z. A., Riedi, P. C., and Tunstall, D. P., "Radiofrequency Echoes in Metallic Powders", J. Phys. F: Metal Phys., 3, 1843 (1973).

17. Powdered specimen of IN-100 was supplied by Mr. A. M. Adair of AFML at the request of Dr. Michael Buckley of DARPA.

18. Drain, L. E., "Nuclear Magnetic Resonance in Metals", Met. Rev., 12, No. 119, 1967.

19. Rowland, T. J., and Fradin, F. Y., "Nuclear Magnetic Relaxation and Atomic Diffusion in Aluminum Alloys", Phy. Rev. 182, No. 3, pp. 760-770, 1969.

20. Leisure, R. G. and Bolef, D. I., "CW Microwave Spectrometer for Ultrasonic Paramagnetic Resonance", Rev. Sci. Instrum. 39, 199 (1968).

21. Hsu, D. K., Leisure, R. G., and Seiber, B. A., "Anomalous Nuclear-Acoustic-Resonance Signals in Aluminum," Phys. Rev. B, 11, No. 11, 4106-9 (1975).

22. Ozimek, E. J., Hsu, D. K., and Leisure, R. G., "Nuclear Acoustic Resonance in Aluminum in the Intermediate Temperature Region", Phys. Rev. B, 18, No. 3, 1508-1513 (1978).

23. Leisure, R. G. Hsu, D. K., and Seiber, B. A., "Nuclear-Acoustic-Resonance Absorption and Dispersion in Aluminum", Phys. Rev. Lett. 30, 1326 (1973).

24. Fedders, P. A., "Acoustic Magnetic Resonance in Metals Via the Alpher-Rubin Mechanism", Phys. Rev. B8, 5156, (1973).

25. Kanert, O. and Mehring, M., "Static Quadrupole Effects in Dis-Ordered Cubic Solids", in NMR-Basic Principles and Progress, Ed. by Diehl, P., Fluck, E., and Kosfeld, R., Vol. 3, Springer-Verlag, New York, 1971, pp. 1-83.

26. Hall, L. A., Survey of Electrical Resistivity Measurements on 16 Pure Metals in the Temperature Range of 0 to 273K, Nat. Bur. Stand. Tech. Note No. 365, U. S. GPO, Washington, D.C., 1968.

27. Cohn, R. W., Physical Metallurgy, N. Holland Pub. Co., 1970.

28. Sagalyn, P. L., and Hofmann, J. A., "Nuclear Magnetic Resonance in Metallic Single Crystals", Phys. Rev. 127, No. 1, pp. 68-71 (1962).

29. Abragam, A., The Principles of Nuclear Magnetism, Clarendon Press, London, 1961, Chapter III.

30. Pawlek and Rogalla, D., "The Electrical Resistivity of Silver, Copper, Aluminum, and Zinc as a Function of Purity in the Range 4-298^{o}K", Cryogenics 6, No. 1, 14-20 (1966) and Metall. 20, No. 9, 949-56 (1966).

31. Thompson, R. B., "New Electromagnetic Transducer Applications", Proc. of the ARPA/AFML Review of Progress in Quantitative NDE, AFML-TR-78-55, May 1978.

APPENDIX

A. Elements of Nuclear Magnetic Resonance

Nuclear Magnetic Resonance (NMR) is based upon the fact that many atomic nuclei in their ground state possess a non-zero spin angular momentum $I\hbar$ and a dipolar magnetic moment $\vec{\mu} = \gamma\hbar\vec{I}$. Here, I denotes the "spin" of the nucleus, and must be an integer or half-integer. The ratio, γ , between the magnetic moment and the angular momentum is a property of the nucleus, and is called the gyromagnetic ratio. In the presence of an externally applied magnetic field, the magnetic dipoles have an energy of orientation given by the eigenvalues of the Zeeman Hamiltonian[1]

$$\mathcal{H}_M = -\vec{\mu}\cdot\vec{H}_o = -\gamma\hbar\vec{I}\cdot\vec{H}_o \tag{A1}$$

where $\vec{H}_o$ is the applied magnetic field. If $\vec{H}_o$ lies along the z direction of the Cartesian coordinate system, the Hamiltonian becomes

$$\mathcal{H}_M = -\gamma\hbar I_z H_o \tag{A2}$$

and the eigenvalues correspond to the $2I + 1$ allowed values of the z component of the angular momentum, $m = -I, -I+1, \ldots, I-1, I$. The energy levels are given by

$$E_m = -\gamma\hbar H_o m \tag{A3}$$

Thus, the effect of the applied field is to give rise to $2I + 1$ equally spaced energy levels with the separation $\gamma\hbar H_o$. If a periodic energy perturbation of frequency ν_o is applied to this system such that

$$h\nu_o = \Delta E = \gamma\hbar H_o \tag{A4}$$

transitions may be induced between adjacent Zeeman energy levels. This is the phenomenon of nuclear magnetic resonance (NMR). Typically for $H_o \approx 10\text{kOe}$, $\nu_o \approx 10$ MHz. In a conventional NMR experiment the energy perturbation consists of a small sinusoidally oscillating magnetic field of amplitude H_1 applied in the x-y plane, usually generated by an rf coil surrounding the specimen. Although the transition probabilities for upward and

---

* Numbers in parentheses refer to the references at the end of this appendix.

downward transitions of a nuclear spin are equal, in thermal equilibrium the lower energy states are preferentially occupied, and this results in more spins moving from lower to higher states than vice versa. This gives rise to a net power absorption per unit volume, P_n, which can be written as[2]

$$P_n = \frac{N h^2 \nu^2 \gamma^2 H_1^2 g(\nu) F(I)}{16 kT} \tag{A5}$$

where

H_1 = amplitude of oscillating rf magnetic field

$g(\nu)$ = line shape factor reflecting width of resonance

$$F(I) = \frac{1}{2I+1} \sum_{m=-I+1}^{I} (I+m)(I-m+1) = \frac{35}{6} \text{ for } Al^{27}$$

Although Equation (A4) suggests a unique relationship between the resonant frequency and the applied field, the actual field "seen" by the various nuclei in a solid material varies from nucleus to nucleus because of dipolar couplings between the spins and other internal interactions, so that the resonance takes place over a range of frequencies centered around ν_o . Thus the observed resonance line possesses a certain frequency width which reflects the internal fields in the specimen.

B. Quadrupole Interactions

Nuclei with a spin I satisfying the condition $I \geq 1$ may have an electric quadrupole moment in addition to a magnetic dipole moment.[3] This electric quadrupole moment reflects the asphericity of the nuclear electrical charge distribution. Since nuclei have no electric dipole moments, they are insensitive to homogeneous electric fields, however, nuclei with quadrupole moments experience interactions with sufficiently inhomogeneous electric fields as might be produced, for example, by the lattice ions surrounding the necleus in question. The Hamiltonian for this interaction for an axially symmetric field gradient may be written.[4]

$$\mathcal{H}_Q = \frac{e^2 q Q}{4I^2(2I-1)} \left[3I_z^2 - I(I+1)\right] \tag{A6}$$

where

Q = static electric quadrupole moment of the nucleus

eq = z-component of the field gradient tensor in the principal axes system

For cubic symmetry, the field gradient equals zero and the quadrupole interaction vanishes.

Thus in the general case for spins $I \geq 1$, the Hamiltonian is a combination of (A1) and (A6)

$$\mathcal{H} = \mathcal{H}_M + \mathcal{H}_Q \tag{A7}$$

The two cases generally considered are those where the Zeeman Hamiltonian, $\mathcal{H}_M$, is either very large or very small compared to the quadrupole interaction energy. In the work discussed here only the case $\mathcal{H}_M \gg \mathcal{H}_Q$ will be considered so that the quadrupole energy may be treated as a perturbation of the Zeeman energy. In this situation, the electric quadrupole interaction manifests itself in the nuclear magnetic resonance spectra through its influence on the parameters of the resonance line, such as intensity and linewidth, central frequency, and on the relaxation of nuclear spins. Figure A1 shows the first order shifting of the Zeeman energy levels due to a quadrupole perturbation for $I = 3/2$.

Although the electric field gradient in general vanishes for perfect cubic symmetry, in ordinary specimens, imperfections can easily cause sufficient local departure from cubic symmetry for quadrupole interactions to have a pronounced effect on the resonance line.[5] In imperfect crystals, electric field gradients might be caused by:[6]

(i) stress-strain fields produced by externally applied loads or lattice defects

(ii) additional charges from point defects with a charge difference with respect to the host ions

(iii) redistribution of conduction electrons around a defect in the case of metals.

In polycrystalline specimens, the electric field gradients associated with imperfections are generally random in orientation and magnitude, so that the quadrupole interaction of these gradients with the nuclei produce a "blurring" or spreading of the Zeeman energy levels resulting in changes in the nuclear resonance lineshape, the specific changes depending on the strength of the quadrupole interaction.

The electric field gradients resulting in case (iii) formed the basis for much important NMR work by Rowland on the study of the electronic

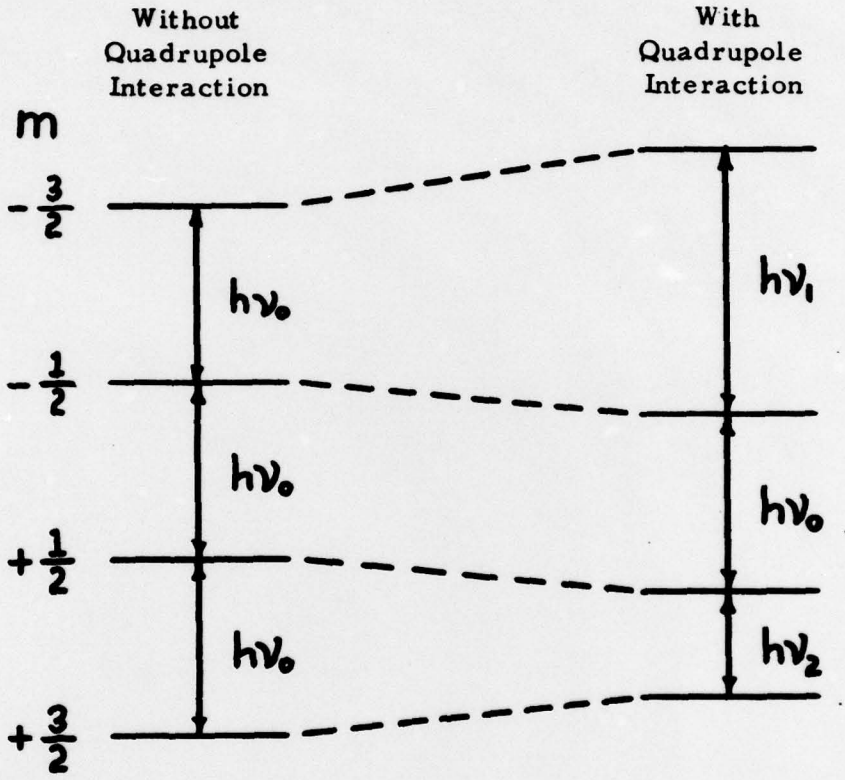

FIGURE A1. QUADRUPOLE PERTURBATION FOR A NUCLEUS OF SPIN $\frac{3}{2}$

structure of various alloy systems in terms of the charge redistributions which occur around impurity atoms.[7] He also demonstrated the effect of internal strains on NMR in metal powders due to cold working,[8] but only recently have detailed theoretical investigations been made of the quadrupole interactions associated with specific lattice defects such as point defects and dislocations.[9] Calculations were made on the effect of random distributions of point defects and specific dislocation structures on NMR lineshapes, relaxation times, and spin echo shapes, and in most cases, good agreement with experiment was found.[10] The theoretical background pertaining to the effect of internal strains on NMR signals via the quadrupole interaction will be discussed in the next Section.

C. Theoretical Analysis of Lattice Strain

As has been previously mentioned, nuclei with a spin $I > 1/2$ may possess an electric quadrupole moment which can interact with an electric field gradient. In a perfect cubic lattice, the quadrupole interaction would ordinarily vanish since the net electric field gradient at each nucleus is zero due to the cubic symmetry. However, lattice defects destroy the cubic symmetry producing local field gradients which cause a quadrupole interaction. The mean quadrupole interaction from all of the nuclei in the sample acts as a perturbation on the NMR line. The quadrupolar interaction associated with point defects, dislocation dipoles, and dislocations has been analyzed theoretically and compared to experiment.[11] Theoretical predictions agree well with the point defect model in the case of underformed specimens, whereas in the case of deformed specimens, the dislocation model is valid. Following Kanert[12], a theoretical discussion is presented of the quadrupole interaction due to dislocations in deformed aluminum.

The NMR absorption line shape function $g(\omega)$ may be written as a superposition of the partial lines $g^{(m)}(\omega)$ which belong to different magnetic energy transitions $m \rightarrow m - 1$

$$g(\omega) = \sum_{m=-I+1}^{I} d_m g^{(m)}(\omega) \tag{A8}$$

where

$$\int_{-\infty}^{+\infty} g(\omega) d\omega = \int_{-\infty}^{+\infty} g^{(m)}(\omega) d\omega = 1$$

and the relative intensity a_m of the line $g^{(m)}(\omega)$ is given by

$$a_m = \frac{(I+m)(I-m+1)}{\sum_{m=-I+1}^{I} (I+m)(I-m+1)} \tag{A9}$$

In the case of a rigid cubic lattice the form of the partial lines $g^{(m)}(\omega)$ is determined (1) by magnetic dipole interaction between nuclear spins; and (2) by interaction between the nuclear quadrupole moments and the local electric field gradients caused by lattice defects. If we let the dipolar portion of the line shape be denoted by $g_D(\omega)$, and the quadrupolar portion (which depends on spin quantum number m) by $g_Q^{(m)}(\omega)$, Eq. (A8) may be rewritten in the case of first-order quadrupole perturbation as

$$g(\omega) = a_{\frac{1}{2}}\, g_0(\omega) + \sum_{m=3/2}^{I} 2\, a_m\, g_0(\omega) * g_Q^{(m)}(\omega) \tag{A10}$$

where

$$\int_{-\infty}^{+\infty} g_0(\omega)\, d\omega = \int_{-\infty}^{+\infty} g_Q^{(m)}(\omega)\, d\omega = 1$$

and the asterisk (*) stands for the convolution integral between the dipolar and quadrupolar line functions. Substituting a mean line function $g_Q(\omega)$ for $g_Q^{(m)}(\omega)$, we obtain

$$g(\omega) = a_{\frac{1}{2}}\, g_0(\omega) + g_0(\omega) * g_Q(\omega) \sum_{m=3/2}^{I} 2\, a_m \tag{A11}$$

The function $g_Q(\omega)$ produced by strain fields around (111) $\langle 110 \rangle$ dislocations has been calculated and found to have the form[13]

$$g_Q(\omega) = \frac{3\sqrt{3}}{4\pi} \frac{1}{\langle \omega_Q' \rangle} \frac{1}{1 + \left| \frac{\omega}{\langle \omega_Q' \rangle} \right|^3} \tag{A12}$$

where $\langle \omega_Q' \rangle$ is the absolute first moment of the line shape function, and is given by

$$\langle \omega_Q' \rangle = A\sqrt{c} \int_0^{2\pi} |f(\theta, h_i)| \, d\theta \tag{A13}$$

Here, c is the dislocation density, $f(\theta, h_i)$ is an orientation function depending on the type and orientation of the dislocations relative to the magentic field H_o (h_i = direction cosines), and

$$A = \frac{\sum_{m=3/2}^{I} (2m-1) C_m}{\sum_{m=3/2}^{I} C_m} \cdot \frac{3eQ}{4I(2I-1)h} \cdot GbS_{44} \tag{A14}$$

where e = electronic charge, Q = nuclear quadrupole moment, G = shear modulus, b = module of the Burgers vector, and S_{44} = element 44 of the gradient elastic matrix which relates the electric field gradient tensor with the strain tensor.[14]

Measurements in nearly perfect crystals (devoid of quadrupole interactions) show that the NMR line has a Gaussian form to a good approximation. Thus, the dipolar contribution $g_D(\omega)$ in Eq. (A11) may be expressed as

$$g_D(\omega) = \frac{1}{\sqrt{2\pi}} \cdot \frac{1}{\sqrt{\langle \omega_o^2 \rangle}} \exp\left(-\frac{\omega^2}{2\langle \omega_o^2 \rangle}\right) \tag{A15}$$

where $\langle \omega_o^2 \rangle$ is the second moment of the dipolar line function. Substituting the line shape functions given by Eqs. (A12) and (A15) into Eq. (A11) and using the normalized frequency $y = \omega / \sqrt{\langle \omega_o^2 \rangle}$ and the normalized quadrupole perturbation $z = \dfrac{\langle \omega_Q' \rangle}{\sqrt{\langle \omega_o^2 \rangle}}$, Kanert obtains [15]

$$g(y,z) = a_{1/2} \frac{1}{\sqrt{2\pi}} \exp\left(-\frac{y^2}{2}\right) + \frac{3\sqrt{3}}{4\pi\sqrt{2\pi}} z^2 \int_{-\infty}^{+\infty} \frac{\exp\left(-\frac{x^2}{2}\right)}{z^3 + |y-x|^3} dx \sum_{m=3/2}^{I} 2a_m \tag{A16}$$

This is the final expression for the line shape function resulting from quadrupole interactions due to (111) $\langle 110 \rangle$ dislocations. Plotting the relative peak-to-peak intensity f/f_o of the derivative $\frac{d}{dy}\, g(y, z)$ of Eq. (A16), (which is what is actually recorded in continuous wave NMR experiments) as a function of the normalized quadrupole perturbation z, results in the graph shown in Figure A2 for $I = 5/2$ (the nuclear spin of aluminum). As expected, the relative intensity $\frac{f}{f_o}$ decreases from one to $a_{1/2}$ with increasing perturbation z.

Although a contribution to the quadrupole interaction may be expected from the redistribution of conduction electron charge distribution which occurs in a metal near a dislocation, this has been shown to have a negligible influence ($< 1\%$) on the signal intensity compared with the quadrupole perturbation due to lattice strain.[16] In the case of charge impurities in metals and alloys, the opposite holds true, namely, the quadrupole interaction is primarily due to the charge redistribution rather than strain effects.[17]

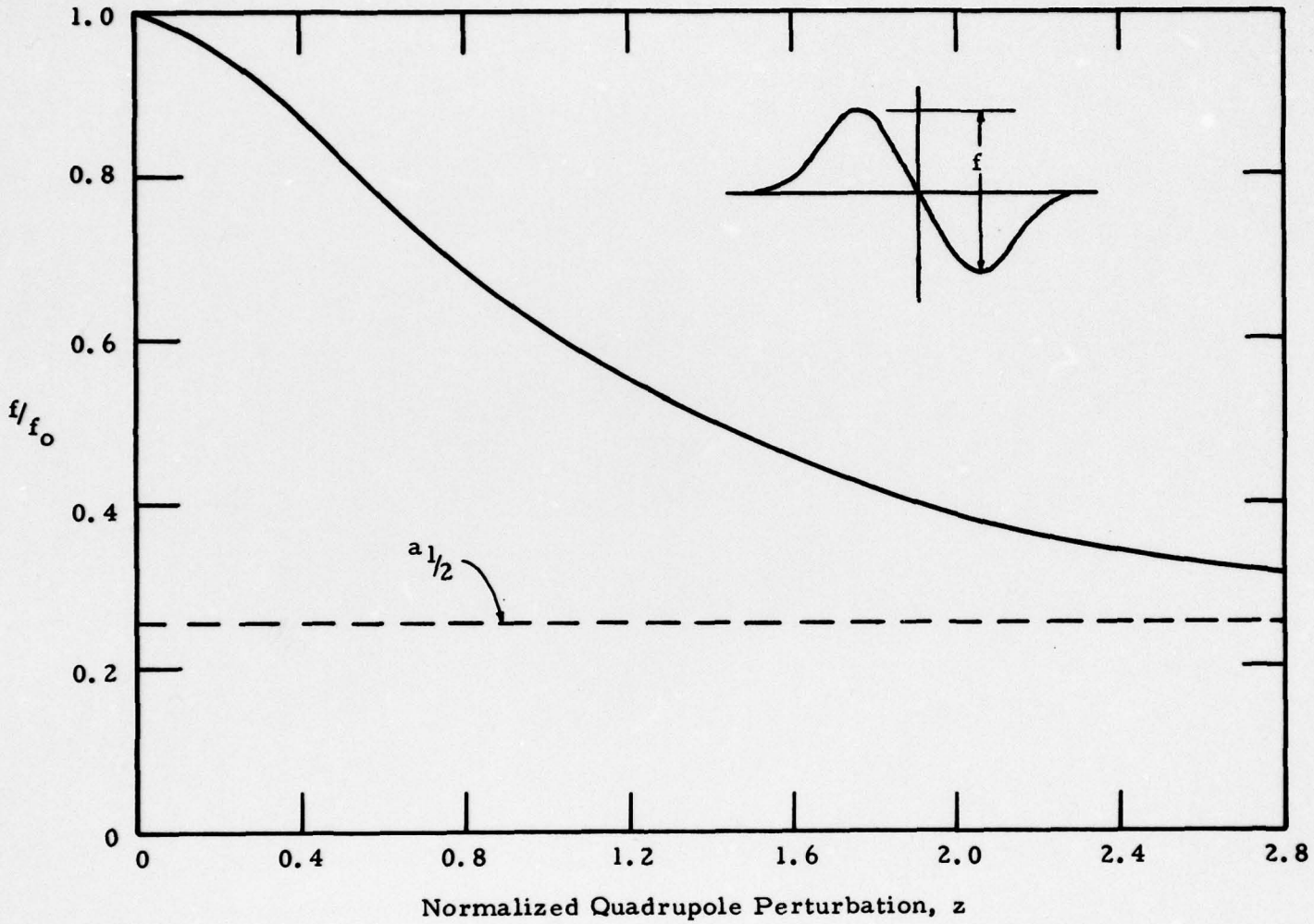

FIGURE A2. NORMALIZED NMR PEAK-TO-PEAK INTENSITY f/f_o VERSUS NORMALIZED QUADRUPOLE PERTURBATION z DUE TO DISLOCATIONS FOR $I = \frac{5}{2}$

REFERENCES

1. Abragam, A., The Principles of Nuclear Magnetism, Clarendon Press, Oxford, 1961.

2. Ibid.

3. Das, T.P., and Hahn, E.L., "Nuclear Quadrupole Resonance Spectroscopy," in Solid State Physics, Ed. by Seitz, F., and Turnbull, D., Suppl. 1, Academic Press, New York, 1958.

4. Ibid.

5. Cohen, M.H., and Reif, F., "Quadrupole Effects in Nuclear Magnetic Resonance Studies in Solids," in Solid State Physics, Ed. by Seitz, F., and Turnbull D., Vol. 5, Academic Press, New York, 1957, pp. 321-438.

6. Kanert, O., and Mehring, M., "Static Quadrupole Effects in Disordered Cubic Solids," in NMR - Basic Principles and Progress, Ed. by Diehl, P., Fluck, E., and Kosfeld, R., Vol. 3, Springer-Verlag, New York, 1971, 11. 1-83.

7. Rowland, T.J., "Nuclear Electric Quadrupole Interactions in Aluminum," Acta Met. 3, 74 (1955). Bloembergen, N., and Rowland, T.J., "On the Nuclear Magnetic Resonance in Metals and Alloys," Acta Met. 1, 731 (1953).

8. Ibid.

9. Kanert, O., Kotzur, D., and Mehring, M., "Influence of Point Defects and Dislocations on the Line Shape of Nuclear Magnetic Resonance Signals," Phys. Stat. Sol. 36, 291 (1969).

10. Kanert and Mehring, op. cit.

11. Ibid.

12. Kanert, O., "Quadrupole Broadening of Nuclear Magnetic Resonance Lines in Deformed Copper and Aluminum," Phys. Stat. Sol. 32, 667 (1969).

13. Kanert, O., "Calculation of Quadrupole Broadening from (111) ⟨110⟩ Dislocations in Cubic Crystals," Phys. Stat. Sol. 30, 127 (1968).

14. Shulman, R.G., Wyluda, B.J., and Anderson, P.W., "Nuclear Magnetic Resonance in Semiconductors. II. Quadrupole Broadening of Nuclear Magnetic Resonance Lines by Elastic Axial Deformation," Phys. Rev. 107, 953 (1957).

15. Kanert, O., "Quadrupole Broadening of Nuclear Magnetic Resonance Lines in Deformed Copper and Aluminum," op. cit.

16. Ibid.

17. Rowland, T.J., "Nuclear Magnetic Resonance in Metals," in Progress in Materials Science, Ed. by Chalmers, B., Vol. 9, Pergamon Press, New York, 1961, pp. 1-91.